

Tuning the Cavity of Cyclodextrins: Altered Sugar Adaptors in Protein Pores

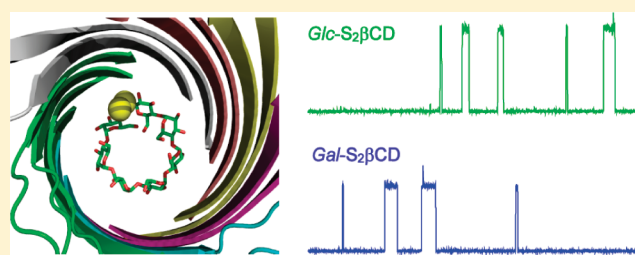
Wen-Wu Li,[†] Timothy D. W. Claridge,[†] QiuHong Li,[†] Mark R. Wormald,[‡] Benjamin G. Davis,^{*,†} and Hagan Bayley^{*,†}

[†]Department of Chemistry, University of Oxford, Chemical Research Laboratory, Mansfield Road, Oxford OX1 3TA, United Kingdom

[‡]Oxford Glycobiology Institute, Department of Biochemistry, University of Oxford, South Parks Road, Oxford OX1 3QU, United Kingdom

 Supporting Information

ABSTRACT: Cyclodextrins (CDs) have been widely used in host–guest molecular recognition because of their chiral and hydrophobic cavities. For example, β -cyclodextrin (β CD) lodged as a molecular adaptor in protein pores such as α -hemolysin (α HL) is used for stochastic sensing. Here, we have tuned the cavity and overall size of β CD by replacing a single oxygen atom in its ring skeleton by a disulfide unit in two different configurations to both expand our ability to detect analytes and understand the interactions of β CD with protein pores. The three-dimensional structures of the two stereoisomeric CDs have been determined by the combined application of NMR spectroscopy and molecular simulation and show distorted conformations as compared to natural β CD. The interactions of these synthetic β CD analogues with mutant α HL protein pores and guest molecules were studied by single-channel electrical recording. The dissociation rate constants for both disulfide CDs from the mutant pores show \sim 1000-fold increase as compared to those of unaltered β CD, but are \sim 10-fold lower than the dissociation rate constants for β CD from wild-type α HL. Both of the skeleton-modified CDs show altered selectivity toward guest molecules. Our approach expands the breadth in sensitivity and diversity of sensing with protein pores and suggests structural parameters useful for CD design, particularly in the creation of asymmetric cavities.



INTRODUCTION

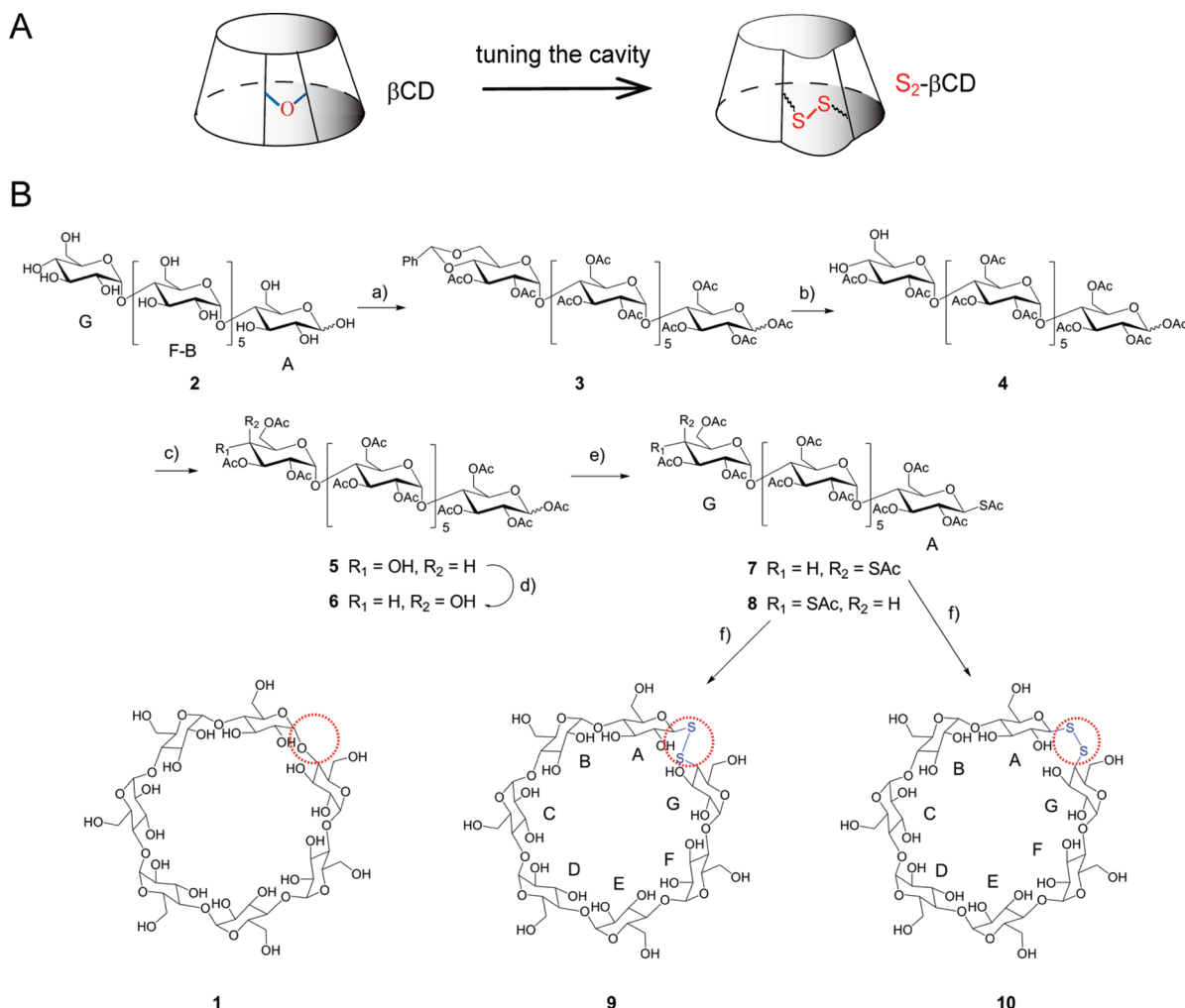
Cyclodextrins (CDs) are cyclic oligomers of α (1 \rightarrow 4)-linked D-glucopyranose units. The glucose residues of CDs are arranged in a doughnut-shaped structure with a hydrophilic exterior and a hydrophobic cavity that allows the formation of host–guest inclusion complexes with hydrophobic molecules.^{1–3} Because of the unique properties of CDs, they have been used in the pharmaceutical industry;⁴ for example, a modified CD, sugammadex, is used to reverse neuromuscular blockade by rocuronium.⁵ CDs also have been used for the construction of CD-based supramolecular assemblies,^{6–8} such as rotaxanes and catananes, and for the manipulation and modification of DNA^{9,10} and enzymes.¹¹ In addition, nanopore detection is an emerging technology for the stochastic sensing of a large range of molecules,^{12,13} which also uses CDs. In particular, a heptameric transmembrane protein pore (α -hemolysin, α HL) assembled from seven copies of a 293 amino acid polypeptide¹⁴ has been used for the detection of metal ions,¹⁵ proteins,¹⁶ DNA,¹⁷ and organic molecules through both noncovalent¹⁸ and covalent^{19–21} binding interactions. The use of CDs as molecular adaptors in such protein pores expands their ability to sense molecules.^{22–25} For example, β -cyclodextrin (β CD, 1) (Scheme 1), a molecule

with C_7 symmetry, has been lodged at sites within the lumen of the wild-type (WT) and mutant α HL pores.^{26,27} These α HL pore- β CD complexes can be used to detect various analytes by single-channel electrical recording. Crystal structures of the heptameric ($M113N$)₇ and ($M113F$)₇ mutants with bound β CD (Figure 1) have recently revealed key interactions between β CD and mutant α HL pores.²⁸ On the basis of these structures, modified β CDs have also been covalently attached to the pore to improve stochastic sensing.²⁹ Moreover, substituent-modified CDs such as heptakis-(6-deoxy-6-amino)- β -cyclodextrin have been used as noncovalent²⁵ and covalent³⁰ adaptors within the α HL pore to differentiate deoxynucleotides with potential application in DNA sequencing.

Despite the successful use of natural and modified CDs as adaptors, we considered that ring skeleton-modified CDs would provide novel adaptors with cavities of different diameter, symmetry, and/or shape, and therefore significantly modulate host–guest molecular recognition. Such ring skeleton alterations are rare. Previously, a thioether,³¹ aromatic spacers,^{32,33} a hexa-2,5-diyne-1,6-dioxy unit,³⁴ a β -1,4 rather than α -1,4 glycosidic

Received: November 10, 2010

Published: January 18, 2011

Scheme 1. Strategy for Tuning the Cavity of β CD^a

^a (A) Cartoon presentation of the creation of an asymmetric S₂βCD with a "bulge". Replacement of a glycosidic oxygen atom of βCD by a disulfide unit could yield four stereoisomers through variation of the stereochemistry of the anomeric position (α or β) and C-4 of the terminal sugar unit (gluco- or galacto- configuration). (B) Chemical synthesis of two S₂βCD both with a β-thiol at C-1A but different configurations at C-4G, Glc-S₂βCD (9), and Gal-S₂βCD (10). Reagents and conditions: (a) (i) α,α-dimethoxytoluene, *p*-toluenesulfonic acid monohydrate, DMF, 50 °C, 16 h; (ii) acetic anhydride, pyridine, 80 °C, 2 h, yield over two steps 22%; (b) 80% HOAc, 50 °C, 8 h, yield 37%; (c) 1-acetoxybenzotriazole/triethylamine/DCM, room temperature, 17 h, yield 74%; (d) (i) Tf₂O, pyridine, DCM, -10 °C, 1 h, then room temperature, 3 h; (ii) NaNO₂, DMF, 50 °C, 6 h, yield over two steps 50%; (e) (i) Tf₂O, pyridine, DCM, -10 °C, 1 h, then room temperature, 2 h; (ii) 33% HBr/HOAc, room temperature, 5 h; (iii) KSAc, DMF, room temperature, 16 h; overall yield 19% and 18% for 7 and 8, respectively; (f) NaOMe, MeOH, under air, room temperature, 24 h; 9 (12%) and 10 (11%).

linkage,³⁵ and a triazole moiety^{34,36} have been used as linkages to create cyclic variants of linear sugars. An extended linkage containing a disulfide bond has also been placed into a methylated CD.³⁷ Interestingly, some of these skeleton-modified CDs have shown altered inclusion selectivity toward guest molecules.^{31,35–38} However, direct replacement of the glycosidic linkage with a disulfide bond in CDs has not been previously accomplished. Insertion of this short motif and variation of the configuration of the disulfide bond could create a library of four stereoisomers as βCD analogues (S₂βCD) with subtly altered cavities and symmetries (Scheme 1A). In addition, such S₂βCDs would have the potential for reversible cyclization through a bond-forming process that could be accomplished under aqueous, benign conditions.³⁷ We considered that such precisely altered CDs would help us understand the structure–activity relationships of the interactions between analytes, CDs, and

protein pores. Here, we report the chemical synthesis and NMR-derived three-dimensional structures of two ring-expanded, disulfide-linked stereoisomeric CDs. We use single-channel recording to examine their interactions with mutant αHL protein pores and determine the kinetics of host–guest molecular recognition.

RESULTS

Chemical Synthesis of Two Altered Cyclodextrins. The insertion of an additional atom (1 O atom → 2 S atoms) into the backbone of βCD allowed subtle expansion of the cavity diameter and was achieved by the creation of two disulfide-linked analogues 9 and 10 (Scheme 1B), in which the glycosidic bond (α-C–O–C) between ring A and G was replaced by a disulfide linkage (β-C–S–S–C) either with overall retention of configuration at C-4 of ring G (9) or inversion (10). The

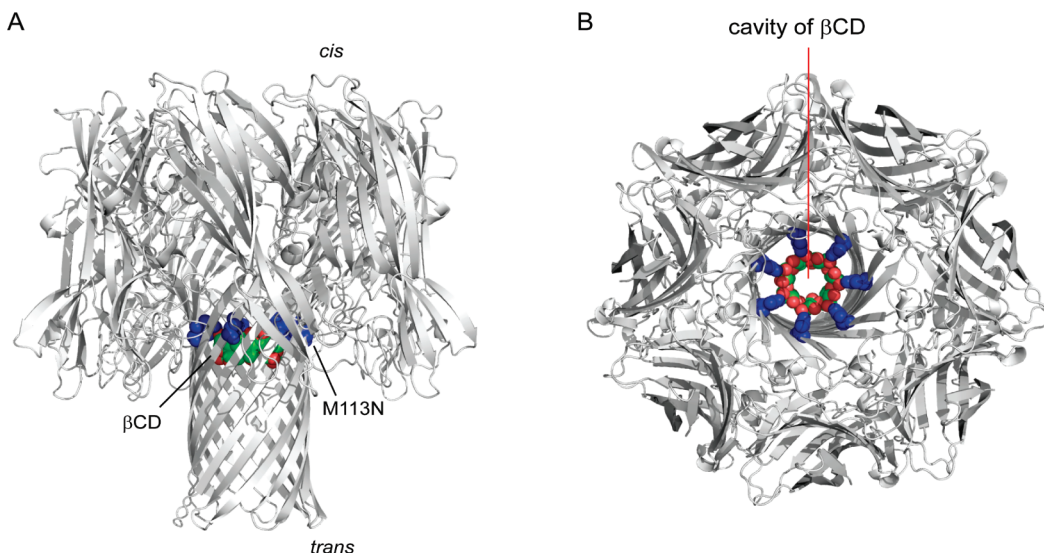


Figure 1. X-ray structure of $(M113N)_7 \alpha\text{HL}$ pore with bound βCD (rendered from PDB code 3M4E by PyMol). (A) A side view of the structure of $(M113N)_7 \cdot \beta\text{CD}$. αHL is shown in cartoon form (gray). The side chains of the seven Asn-113 residues (blue) and βCD (oxygen, red; carbon, green) are shown as space-filling models. (B) A view down the 7-fold axis from the top, or cis, side of the structure of $(M113N)_7 \cdot \beta\text{CD}$.

terminal 4,6-diol unit of linear maltoheptasaccharide **2** was first protected as its benzylidene acetal, and the product was peracetylated to give **3**. Careful acid hydrolysis of the 4,6-benzylidene group yielded diol **4**. Selective acetylation of the free 6-hydroxy group³⁹ of **4** gave the key intermediate **5** and allowed selective access to OH-4 of the nonreducing terminal residue. The configuration of the equatorial OH-4 of **5** was first inverted through NaNO_2 -mediated substitution of the corresponding triflate and subsequent hydrolysis^{40,41} to give compound **6** with a *galacto*-configuration in the nonreducing sugar unit. This assignment was supported by a shift of the ^1H NMR signal at δ_{H} 3.54 ppm (1H, t, $J = 9.7$ Hz, H-4G) of the *gluco*-configured **5** to δ_{H} 4.00 ppm (1H, m, H-4G) of the *galacto*-configured **6**. Triflation of the 4-hydroxy group of the nonreducing unit of **5**, followed by creation of the anomeric bromide of the reducing unit and subsequent treatment with thioacetate, allowed concomitant displacement of both triflate and bromide to give the acetyl maltoheptasaccharide **7**, possessing a thioacetyl group at both C-1A and C-4G. Application of the parallel transformation to **6** allowed synthesis of the epimeric bis-thioacetate (**8**) in which sulfur was introduced with overall retention of configuration of C-4G. The ^{13}C NMR signals from C-4G of **7** and **8** [δ_{C} 46.63 (d, C-4G) and 43.60 (d, C-4G) ppm, respectively] were consistent with similarly configured structures, for example, 4-*thiogalacto*⁴² and 4-*thiogluco*⁴⁰, respectively. The ^{13}C NMR signals from C-1A of **7** and **8** (both at $\sim\delta_{\text{C}}$ 80 (d, C-1A) ppm) were also consistent with those of similar structures reported previously.⁴³ Final Zemplén deacetylation of **8** and **7** with NaOMe in MeOH led to not only the complete removal of the acetyl groups but also the respective formation of cyclic oligosaccharides **9** and **10** by disulfide bond formation through air oxidation. Compound **9** is a *gluco*-configured disulfide analogue of βCD (termed $\text{Glc-S}_2\beta\text{CD}$) but differs from βCD at C-1A; it is a stereoisomer (epimer) of **10**, which has the *galacto*-configuration (termed $\text{Gal-S}_2\beta\text{CD}$) (see Figure S1 for further details).

Structural Analysis of $\text{Glc-S}_2\beta\text{CD}$ (9**) and $\text{Gal-S}_2\beta\text{CD}$ (**10**).** The structures of $\text{Glc-S}_2\beta\text{CD}$ (**9**) and $\text{Gal-S}_2\beta\text{CD}$ (**10**) were investigated by ^1H NMR (Figure 2), 1D (Figure S2) and 2D

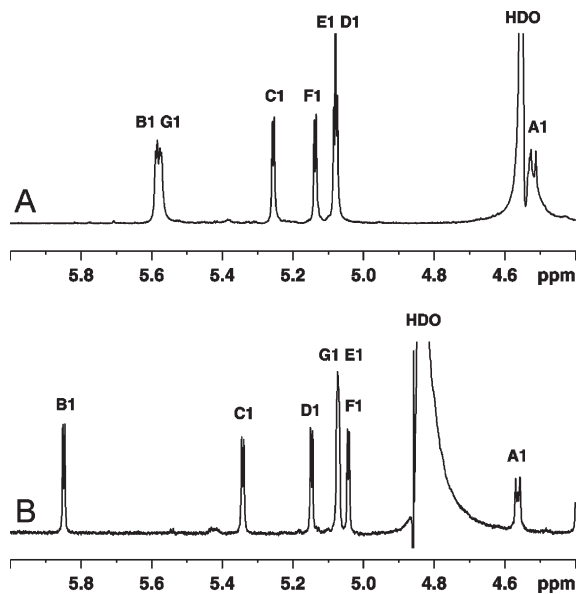


Figure 2. 700 MHz ^1H NMR spectra of the seven anomeric proton signals of $\text{Glc-S}_2\beta\text{CD}$ (**9**) and $\text{Gal-S}_2\beta\text{CD}$ (**10**). (A) ^1H NMR spectrum of **9** in D_2O at 322 K; (B) ^1H NMR spectrum of **10** in D_2O at 292 K.

TOCSY, 1D (Figure S3) and 2D NOESY, 2D Tr-ROESY, $^1\text{H}-^{13}\text{C}$ HSQC (Figure S4), and $^1\text{H}-^{13}\text{C}$ HMBC spectra. Resonance assignments within each sugar ring were derived initially from 1D and 2D TOCSY spectra by identifying correlations arising from the anomeric protons, with associated carbon assignments established from HSQC data. The distinctive ^1H and/or ^{13}C chemical shift values for C-1A and C-4G due to the sulfur substituent enabled ready sequence assignment for these rings. Subsequent sequential ring assignments were established via NOE correlations from anomeric protons across the glycosidic linkages, with HMBC correlations providing additional evidence for inter-ring connectivity. The complete assignments of protons and carbons are shown in Tables S1 and S2,

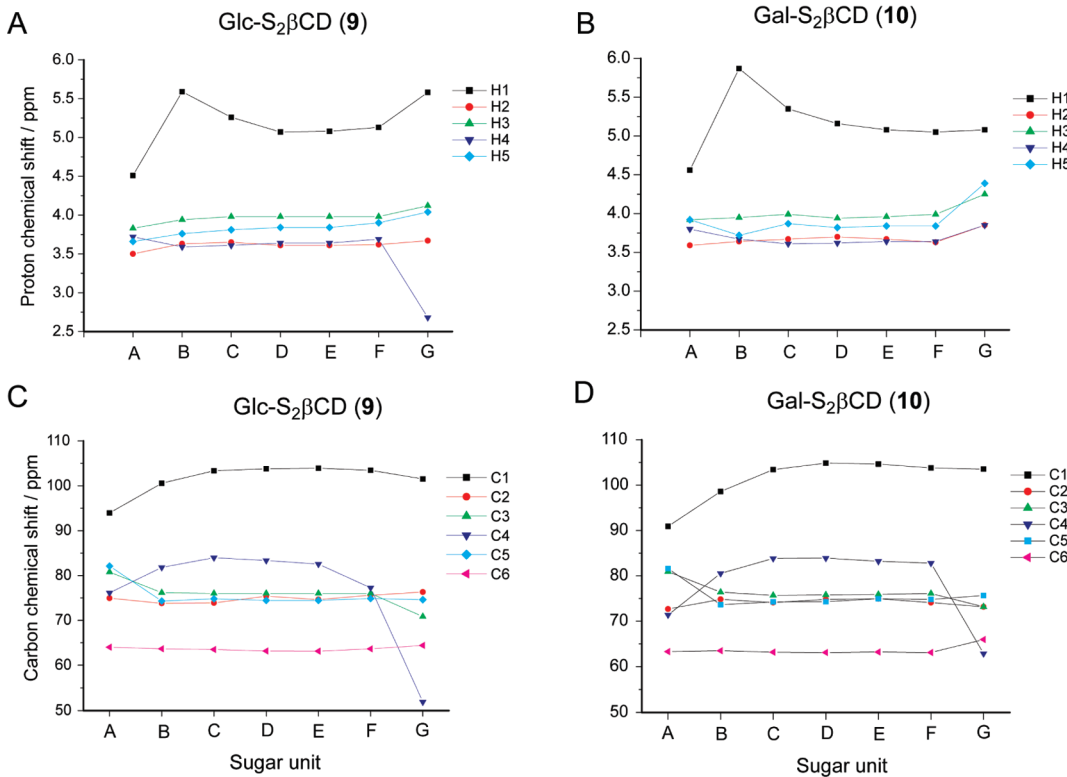


Figure 3. Relationships between the ¹H and ¹³C chemical shifts of each monosaccharide unit in Glc-S₂βCD (**9**) and Gal-S₂βCD (**10**). (A) Comparison of ¹H chemical shifts of H1–5 of each monosaccharide unit in Glc-S₂βCD. (B) Comparison of ¹H chemical shifts of H1–5 of each monosaccharide unit in Gal-S₂βCD. (C) Comparison of ¹³C chemical shifts of C1–6 of each monosaccharide unit in Glc-S₂βCD. (D) Comparison of ¹³C chemical shifts of C1–6 of each monosaccharide unit in Gal-S₂βCD.

Table 1. Experimental Distances of Adjacent Protons from NOE and Heteronuclear Long-Range Coupling Constants (³J (H-1, C-4'), Hz) of Glc-S₂βCD (9**) and Gal-S₂βCD (**10**)^a**

linkage	Glc-S ₂ βCD (9) (322 K)		Gal-S ₂ βCD (10) (292 K)			βCD (1)		
	distance (Å)		distance (Å)	measured ³ J (Hz)	angle θ (deg) ^f	distance (Å)	measured ³ J (Hz)	angle θ (deg)
1B–4A	2.7		~3.1 ^c	<2 ^e	55–120	2.1–2.2	5.3	10–20
1B–3A			~3.1 ^c					
1C–4B	2.2		~2.3 ^d	3.9	~34 ^g			
1D–4C	2.3		2.3	5.0	~15 ^g			
1E–4D	~2.3 ^b		2.3	5.2	~15 ^g			
1F–4E	~2.3 ^b		2.3	5.2	~15 ^g			
1G–4F	>2.5		2.3	5.0	~15 ^g			
1A–3G	3.4							

^a Distance and dihedral angle (θ : H1–C1–O–C4') data for βCD (**1**) are taken from X-ray structures (after addition of protons). ^b Spectrum overlap prevents accurate quantification, but strong NOEs are observed. ^c Weak NOEs, distances approximate. ^d H-2C and H-4B are overlapped, but a strong H-1C and H-4B NOE can be observed. ^e Weak HMBC cross-peak observed. ^f Only absolute magnitudes of the dihedral angle can be determined; signs may be positive or negative. ^g Values of ~5–10° higher are predicted from a theoretically derived Karplus equation.⁵³

respectively. The stereochemistry of the sugar units including sulfur substitution, the differing patterns of ¹H and ¹³C chemical shifts of each sugar unit (Figure 3), interproton distances between adjacent sugar units derived from NOEs, and *trans*-glycosidic dihedral angles from ³J_{C,H} scalar coupling constants (Table 1) were extensively explored to reveal the conformational preferences of **9** and **10** in solution.

The ¹H NMR resonances corresponding to the seven anomeric protons in Glc-S₂βCD (**9**) (Figure 2A) at 322 K and Gal-S₂βCD (**10**) (Figure 2B) at 292 K were partially resolved and

ranged from δ_{H} 4.4 to 6.0 ppm, in contrast to one doublet peak observed for the symmetric βCD (**1**). Among them, the doublets at δ_{H} 4.51 ($J_{1,2}$ = 9.7 Hz) in **9** and 4.56 ppm ($J_{1,2}$ = 8.8 Hz) in **10** can be identified as arising from protons with the β-D-configuration by virtue of the larger coupling constants, and the lower chemical shifts indicating the anomeric carbons to be substituted by sulfur. The other six doublets with smaller coupling constants ($J_{1,2}$ = 3–4 Hz) seen for **9** and **10** indicate the presence of six sugar components with the α-D-configuration. The resonances for H-1 of both rings B and G in **9** in the 1D spectrum are

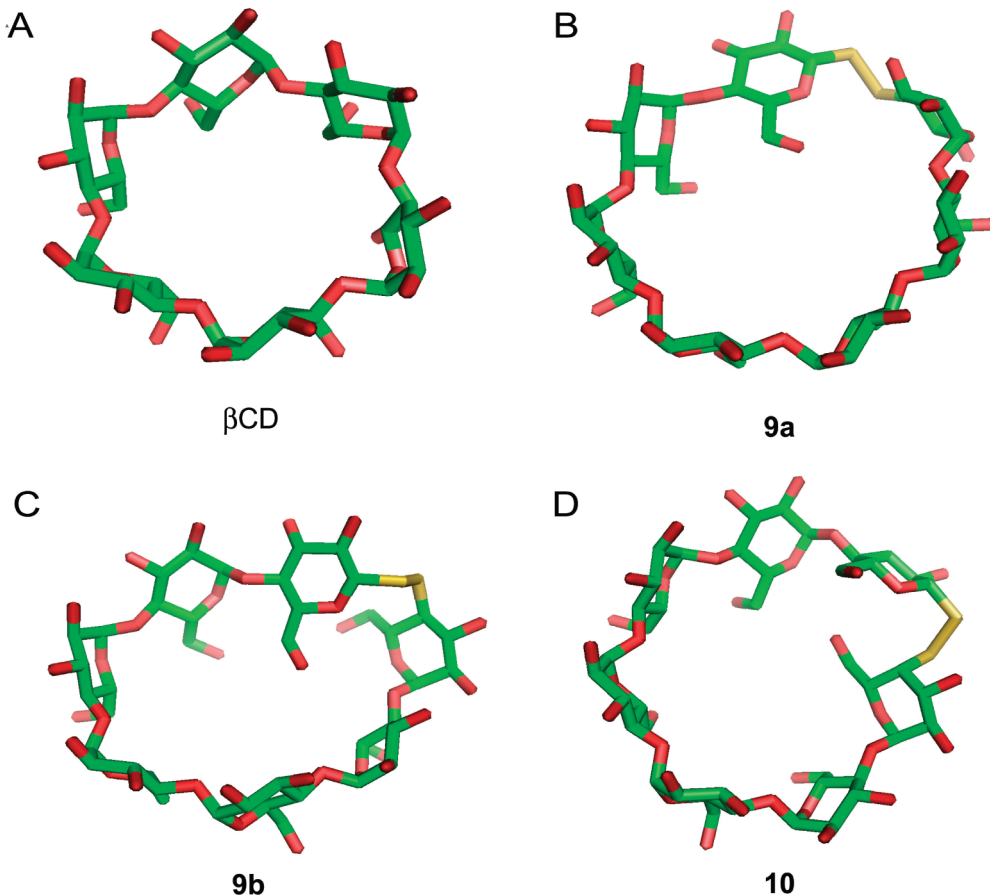


Figure 4. Three-dimensional structure of β CD (**1**), Glc- $S_2\beta$ CD (**9**), and Gal- $S_2\beta$ CD (**10**). Image A for β CD is taken from a structure determined by X-ray crystallography, and the others are from restrained molecular dynamics simulations. All views through the cavity are from the secondary hydroxyl faces of the CDs. (A) Crystal structure of β CD (**1**);⁵⁴ (B) Structure of Glc- $S_2\beta$ CD (**9**) in the -12° anomeric conformation (conformer a, **9a**); (C) Structure of Glc- $S_2\beta$ CD (**9**) in the $+68^\circ$ anomeric conformation (conformer b, **9b**); and (D) Structure of Gal- $S_2\beta$ CD (**10**) in the $+65^\circ$ anomeric conformation. All are shown as stick models (oxygen, red; carbon, green; and sulfur, yellow).

unusually shifted to δ_H 5.59 and 5.58 ppm, while the other anomeric protons show shifts similar to those of β CD (Table S1). However, the signal of H-1 in ring B of **10** is significantly deshielded (to 5.87 ppm), suggesting that conformational differences exist between **9** and **10**. Furthermore, in contrast to the 1H NMR spectrum of **10**, which shows sharp anomeric resonances at 292 K, the 1H NMR spectrum of **9** at this temperature shows a broad peak at δ_H 5.63 ppm for the two overlapping B and G anomeric protons. On increasing temperature from 292 to 322 K, these broad resonances become sharper and can be further distinguished (Figure S5). This suggests the influence of restricted conformational dynamics in **9**, leading to intermediate exchange rates on the NMR chemical shift time scale, which are not observed for **10** or β CD (**1**).

The 1H and ^{13}C chemical shifts of each sugar unit in Glc- $S_2\beta$ CD (**9**) and Gal- $S_2\beta$ CD (**10**) show different patterns (Figure 3). As expected, significant differences between **9** and **10** occur for ring G due to the opposite disulfide stereochemistry at C-4G. Thus, the 1H NMR signals at δ_H 4.04 (m, H-5G), 2.68 (t, $J = 10.6$ Hz, H-4G), and 4.12 (t, $J = 10.1$ Hz, H-3G) are assigned to protons in a 4-thioglucosyl unit in **9** (Figure 3A). In contrast, the 1H NMR signals at δ_H 4.39 (m, H-5G), 3.85 (m, H-4G), and 4.25 (dd, $J = 10.1, 4.6$ Hz, H-3G) are assigned to the protons in a 4-thiogalactosyl unit in **10** (Figure 3B). Otherwise, the trends in proton shifts for H-2, 3, 4, 5 in rings B–F in both **9**

and **10** are similar, with the rings C–F region presenting signals similar to that of β CD itself (Table S1). The differences in the anomeric proton shifts of rings B and G for **9** and **10** are again apparent, suggesting the most significant conformational differences between **9** and **10** are localized in the regions of the disulfide linkages.

The ^{13}C NMR chemical shifts of rings A–F in **9** and **10** show similar trends (Figure 3C and D), with the differences that are observed for ring G ascribed to the differing C4 stereochemistry. Similarly, the C-1A signal in both **9** and **10** exhibits a low shift, large $^3J_{HH}$ coupling constant, and low $^1J_{CH}$ value,⁴⁴ consistent with β substitution by sulfur. However, in **10**, the notable decrease in ^{13}C chemical shifts of C1, C4, and, to a lesser degree, C2, for rings A and B (Figure 3D), together with the larger $^1J_{C-H}$ for ring B, suggests deformation exists about the linkage between these rings. Thus, C-1B is shifted to a low value of δ_C 98.59 ppm ($^1J_{C-H}$, 180 Hz), and C-4A shifted to the low value of 71.38 ppm (Table S2). The ^{13}C NMR of **9** presents a slightly differing picture of distortion about the disulfide bond from that of **10**. While the reduction in the C1 chemical shifts of rings A and B is less than those of **10**, there is evidence in this case that rings F and G are involved in conformational distortion wherein C-4F exhibits a significantly lower chemical shift than in **10**. Thus, C-1B and C-1G in **9** appear at δ_C 100.55 and 101.53 ppm, respectively, and C-4F is reduced to 77.26 ppm (Table S2,

Figure 3C). This suggests that there is deformation about the linkage between rings F and G as well as between rings A and B, relative to the conformations found in β CD. Overall, the trends in chemical shifts indicate differing conformations in the vicinity of the disulfide bridges between **9** and **10**. For both CDs, the rings C, D, and E of the macrocycles resemble unmodified β CD, whereas differences arise for the A–B and F–G linkages for **9** but appear to be concentrated primarily on the A–B linkage in **10**. Such localized conformational deformations may be similar to those found in the crystal structures for some larger CDs with 10, 14, and 26 glucoses as well as methylated α , β , and γ -CDs,⁴⁵ which all possess a rotated glucosyl unit in their structures.^{46–48} Together, these data suggest a successful asymmetric alteration of both the conformation and the cavity of β CD, as intended.

To gain further insight into the conformational differences between **9** and **10** relative to that of β CD (**1**), investigations were extended to consider interproton distances derived from NOEs^{49,50} and *trans*-glycosidic dihedral angles from $^3J_{C,H}$ scalar coupling constants^{51–53} (Figure S6 and the Supporting Information). The resulting distances and angles across the glycosidic linkages in **9** and **10** are listed in Table 1. In the analyses of **9**, a slightly extended distance between H-1B and H-4A of ~ 2.7 Å indicates that the spatial relationship between rings B and A has been distorted and that these two sugar rings are twisted relative to the conformations found between other sugars in **9** and those in β CD.⁴⁶ There also exists a NOE correlation of H-3G to H-1A, which suggests the proximity of rings A and G in **9**. Furthermore, the observation that the NOE between H-1G and H-4F is rather weak (>2.5 Å; estimated due to peak overlap) indicates slight distortion about the F–G linkage, consistent with the chemical shift data (Figures 2A, 3A,C, Tables S1 and S2). The sequential NOEs between the anomeric proton and H-4 in the adjacent sugars of the rings C, D, E, and F of **9** show strong correlations (H-1–H4 distances ~ 2.3 Å), indicating that the relative conformations of these sugar rings are similar to those in β CD, again consistent with predictions from chemical shift data (Figure 3 and Tables S1 and S2).

For **10**, the distances between H-1B and H-4A and between H-1B and H-3A are both around 3.1 Å, indicating a substantial twist to the linkage between rings A and B relative to a β CD linkage. Likewise, the $^3J_{COCH}$ C-4A to H-1B coupling constant is estimated to be less than 2 Hz, which indicates a dihedral angle θ in the range of 55–120° (Table 1) and significantly greater than that typically found for β CD in crystal structures (around 10–20°).⁵⁴ These data are consistent with the unusual 1H and ^{13}C NMR chemical shifts of ring B in **10** (Figure 3, Tables S1 and S2). A slightly twisted angle between rings C and B is also found ($\theta \approx 30^\circ$). A lack of NOEs between protons on rings A and G indicates that these remain predominantly apart in **10**, in contrast to their approach in **9**. The sequential NOEs between the anomeric proton and H-4 in the adjacent sugars of the rings C, D, E, and F of the macrocycle again show strong correlations (distances ~ 2.3 Å). The C-4 to H-1 $^3J_{COCH}$ value (around 5.2 Hz) is similar to 5.3 Hz measured by us for β CD (5.2 Hz, reported in the literature⁵⁵), which also suggests the absence of large torsion angles. These data clearly demonstrate that the sugar rings C, D, E, and F of **10** have relative orientations similar to those in β CD; these conclusions are also in agreement with chemical shift considerations (Figures 2B, 3B,D, Tables S1 and S2).

Molecular Dynamics. To further explore the differing conformational dynamics of **9** and **10**, we undertook molecular

dynamics calculations of both systems to explore the range of conformations adopted by **9** and **10** that are consistent with the observed NOEs. These were performed as restrained molecular dynamics simulations at 300 K in vacuo.

Initial models were generated by using the β CD crystal structure⁵⁴ (Figure 4A) as a template for dynamic simulation. This structure has linkage conformations in the region of ϕ (O5–C1–O–C4) +110° and φ (C1–O–C4–C3) +120°. Here, a ϕ angle correlates with a glycosidic torsion θ angle by $\theta \approx 120^\circ - \phi$. There have been no theoretical studies of the exoanomeric effect for β -dithio-glycosidic linkages, and so no additional terms were explicitly included in the calculation for this torsion angle term. An ordinary β -glycosidic linkage shows energy minima⁵⁶ at a ϕ angle (O5–C1–O–Cx') of -60° and $+60^\circ$, and so separate simulations were started with the A–G linkage ϕ angle (O5–C1–S–S) at either one of these values for both compounds. Constraints were added for all observed cross-linkage NOEs (Table 1), except for the A–G linkage. Some higher temperature simulations (600 K) were also performed on **10**, and additional constraints were added to retain the 4C_1 ring geometries.

Glc-S₂ β CD (**9**) showed two stable conformations (average structures shown in Figure 4B and C) during the simulations, with transitions occurring between these states (Figure S7). The only linkage that differs significantly in conformation between the two states is the A–G linkage, which adopts ϕ values of around -10° in one (conformer a, **9a**, Figure 4B) and $+70^\circ$ in the other (conformer b, **9b**, Figure 4c). Both of these conformers are fully consistent with the NOE constraints used in the simulations, although both predict a longer 1A–3G distance (3.5 and 4.5 Å for **9a** and **9b**, respectively). The discrepancies are likely due to underestimated distances from the weak NOEs. Most of the Glc α 1–4Glc linkages adopt conformations in the region of $\phi:\varphi 110^\circ \pm 10^\circ:120^\circ \pm 10^\circ$ in both conformers, and hence they are similar to those found in β CD, except for the B–A linkage in **9a**, which adopts a 80°:90° conformation and the B–A and G–F linkages in **9b** that adopt a 90°:95° conformation and 140°:140° conformation, respectively. These localized differences are reflected in the experimental 1H and ^{13}C chemical shift data (Figures 2A, 3A,C, Tables S1 and S2). The cavity within **9b** is slightly smaller than that in **9a** because of the displacement of ring A toward the center of the CD ring. Thus, the molecular dynamics simulations suggest that **9** may adopt two global conformations, which can undergo interconversion, with changes in the local B–A, A–G, and G–F linkage conformations occurring between the two. Such interconversion would also be consistent with the dynamic behavior observed in the temperature dependence of 1H NMR spectra of **9** in which the anomeric resonance line widths of only rings A, B, and G are significantly influenced (Figure S5).

Gal-S₂ β CD (**10**) also showed two stable conformations (Figure S8) during the simulations (Figure S9). However, in this case, the conformation adopted depended on the starting geometry, and no transitions between these two conformations were seen in any of the simulations, even when repeated at 600 K. Again, the two differ primarily in the conformation of the A–G linkage, having ϕ values of around $+60^\circ$ (conformer a, **10a**, Figure 4D) and -70° (conformer b, **10b**, Figure S8). However, in this case, there are also significant differences between other linkages. The E–D, F–E, and G–F linkages and the D–C linkage in **10a** all adopt a $\phi:\varphi 110^\circ \pm 10^\circ:130^\circ \pm 20^\circ$ conformation, while the D–C linkage in **10b** varies from this a

Table 2. Conductance Values of $(M113N)_7$ and $(M113F)_7$, and the Complexes of These Pores with β CD (1), Glc-S₂ β CD (9), and Gal-S₂ β CD (10)^a

α HL-pores	CDs	−40 mV			+40 mV		
		g_p (pS)	g_{pc} (pS)	blockade (%)	g_p (pS)	g_{pc} (pS)	blockade (%)
$(M113N)_7$	β CD	728 ± 15	298 ± 18	59 ± 3	798 ± 36	353 ± 19	56 ± 3.5
	Glc-S ₂ β CD	738 ± 37	228 ± 36	69 ± 5	802 ± 13	240 ± 25	70 ± 3.3
	Gal-S ₂ β CD	731 ± 29	268 ± 10	63 ± 3	812 ± 18	322 ± 4	60 ± 2.0
$(M113F)_7$	β CD	653 ± 22	170 ± 11	74 ± 3	766 ± 16	230 ± 7	70 ± 1.7
	Glc-S ₂ β CD	653 ± 44	134 ± 11	79 ± 6	750 ± 53	142 ± 16	79 ± 5.3
	Gal-S ₂ β CD	647 ± 9	209 ± 2	68 ± 1	776 ± 22	250 ± 5	68 ± 2.0

^a 1 M NaCl, 10 mM sodium phosphate, pH 7.5, in both cis and trans chambers. g_p , conductance of the unoccupied α HL pore; g_{pc} , conductance of the pores occupied by CDs, α HL·CD; and the blocking percentage = 100 × ($g_p - g_{pc}$)/ g_p . The values are the mean ± s.d. from five experiments.

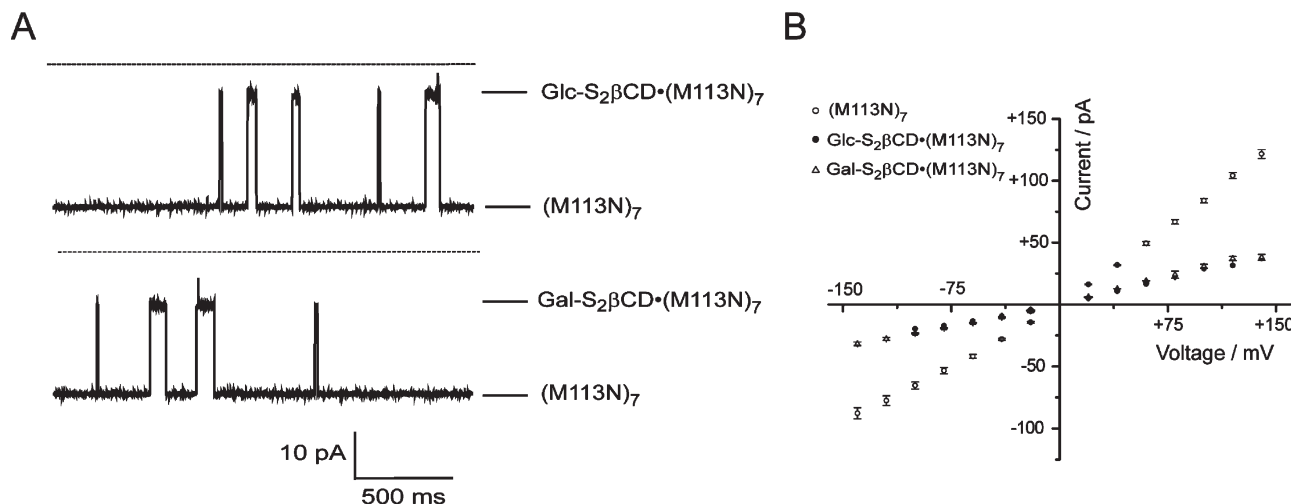


Figure 5. Comparison of the noncovalent binding of Glc-S₂ β CD (9) and Gal-S₂ β CD (10) to the $(M113N)_7$ pore determined by single electrical channel recording. (A) Representative current traces from single α HL pores showing the blockade of $(M113N)_7$ by Glc-S₂ β CD (top) or Gal-S₂ β CD (bottom). The traces were recorded at −40 mV under symmetrical conditions in buffer containing 1 M NaCl, 10 mM sodium phosphate, pH 7.5. Glc-S₂ β CD or Gal-S₂ β CD was added to the trans chamber. The broken line indicates zero current. (B) Single-channel I – V curves for the $(M113N)_7$ pore with and without Glc-S₂ β CD or Gal-S₂ β CD.

little (90°:100°). These are all consistent with the cross-linkage $^3J_{CH}$ coupling constants measured between H1 and C4 of ~5 Hz (Table 1; the corresponding θ angle of ~(−)15° correlates with a ϕ angle of ~105°). However, significant changes are seen in the B–A linkage, 60°:150° in **10b** and 50°:80° in **10a**, and the C–B linkage, 130°:140° in **10b** and 80°:100° in **10a**. The B–A linkage ϕ values of 50° or 60° are both consistent with the cross-linkage $^3J_{CH}$ coupling constant of <2 Hz (Table 1; the corresponding θ angle of ~(−)55 to (−)120° correlates with a ϕ angle range of ~65–0°). The C–B linkage ϕ value of 80° for **10a** is also consistent with the cross-linkage $^3J_{CH}$ coupling constant of 3.9 Hz (Table 1; $\theta \approx (−)34^\circ$ correlates with $\phi \approx 86^\circ$), whereas the value of 130° for **10b** is not. **10a** also provides a better fit to the NOE-derived distances of ~3.0 Å for both 1B–3A and 1B–4A, as compared to 3.5 and 2.5 Å, respectively, for **10b**. Thus, although it is possible from the dynamics simulations that these two conformers may exist, it is apparent that **10a** exhibits greater consistency with the observed NMR data and would appear to be the more likely conformer existing in solution for Gal-S₂ β CD (10). The absence of conformational transitions in the dynamics simulations is also consistent with the lack of evidence for any slow conformational exchange in the 1H NMR spectrum of

Gal-S₂ β CD (10), in contrast to the behavior of Glc-S₂ β CD (9).

Interactions of Glc-S₂ β CD (9) and Gal-S₂ β CD (10) with α HL Mutant Pores. Interactions of Glc-S₂ β CD (9) and Gal-S₂ β CD (10) with α HL heptamic (M113N)₇ and (M113F)₇ pores (preparation and mass spectrometric characterization in the Supporting Information) were investigated by single-channel recording.^{12,22,23} The currents through the pores were monitored under an applied positive or negative potential.^{20,21} Changes in current flow caused by the binding of CDs to the pore and their dissociation were recorded, from which the corresponding rate constants were obtained.^{26,27}

The reversible partial blockades of the single-channel currents were examined by the addition of Glc-S₂ β CD (9) or Gal-S₂ β CD (10) to the trans side of a bilayer containing (M113N)₇. At pH 7.5 and −40 mV, the mean conductance of the pore was reduced from 738 ± 37 to 228 ± 36 pS when Glc-S₂ β CD was bound (M113N₇·Glc-S₂ β CD) and from 731 ± 29 to 268 ± 10 pS when Gal-S₂ β CD was bound (M113N₇·Gal-S₂ β CD) (Table 2 and Figure 5A). At +40 mV, similar current blockades were found (Table 2). Glc-S₂ β CD and Gal-S₂ β CD both show a larger blockade of the conductance of the (M113N)₇ pore as compared to β CD (Table 2) at both −40 and +40 mV. In addition, the blockade of the (M113N)₇ pore by Glc-S₂ β CD is larger than that

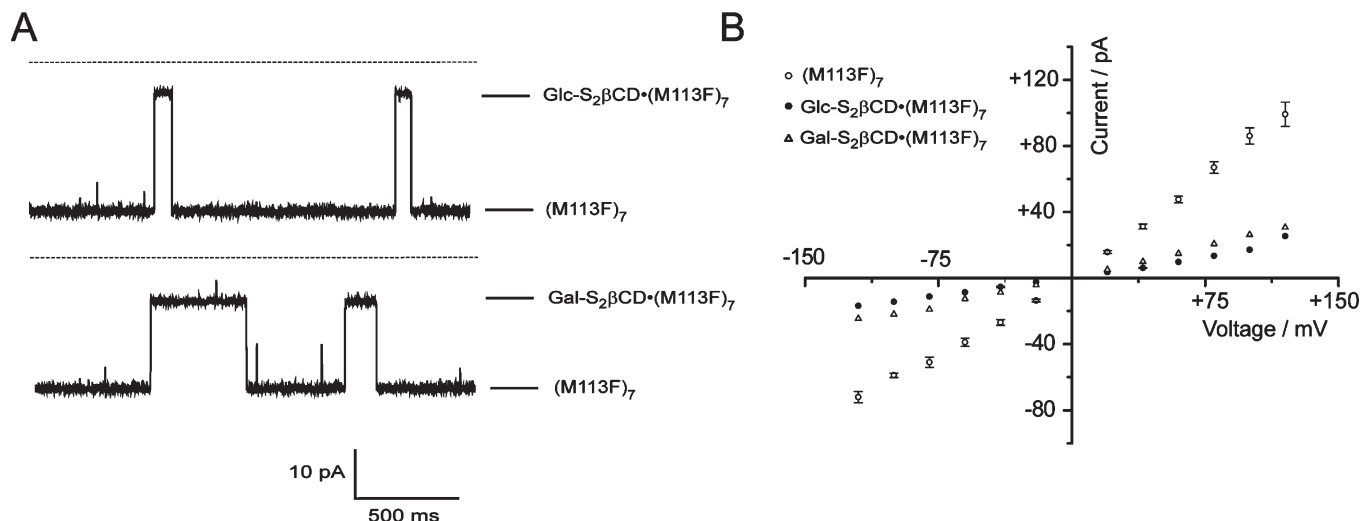


Figure 6. Comparison of the noncovalent binding of Glc-S₂βCD (**9**) and Gal-S₂βCD (**10**) to the (M113F)₇ pore determined by single electrical channel recording. (A) Representative current traces from single αHL pores showing the blockade of (M113F)₇ by Glc-S₂βCD (top) or Gal-S₂βCD (bottom). The traces were recorded at -40 mV under symmetrical conditions in buffer containing 1 M NaCl, 10 mM sodium phosphate, pH 7.5. Glc-S₂βCD or Gal-S₂βCD was added to the trans chamber. The broken line indicates zero current. (B) Single-channel *I*-*V* curves for the (M113F)₇ pore with and without Glc-S₂βCD or Gal-S₂βCD.

Table 3. Kinetic Parameters for the Interactions of βCD (1**), Glc-S₂βCD (**9**), and Gal-S₂βCD (**10**) with the (M113N)₇ and (M113F)₇ Pores**

αHL-pores	CDs	-40 mV			+40 mV		
		<i>k</i> _{on} (M ⁻¹ s ⁻¹) /10 ⁵	<i>k</i> _{off} (s ⁻¹)	<i>K</i> _d (M) × 10 ⁶	<i>k</i> _{on} (M ⁻¹ s ⁻¹) /10 ⁵	<i>k</i> _{off} (s ⁻¹)	<i>K</i> _d (M) × 10 ⁶
(M113N) ₇	βCD ^a	2.7 ± 0.6	0.038 ± 0.011	0.13 ± 0.06	2.9 ± 0.60	0.050 ± 0.008	0.18 ± 0.08
	Glc-S ₂ βCD	1.9 ± 0.2	40 ± 10	210 ± 60 (n = 9)	0.83 ± 0.29	52 ± 9.2	630 ± 200 (n = 9)
	Gal-S ₂ βCD	0.8 ± 0.3	33 ± 13	410 ± 210 (n = 7)	0.54 ± 0.17	53 ± 14	980 ± 400 (n = 7)
(M113F) ₇	βCD ^a	3.1 ± 0.2	0.040 ± 0.007	0.12 ± 0.02	17 ± 3.0	0.086 ± 0.012	0.54 ± 0.02
	Glc-S ₂ βCD	1.4 ± 0.2	23 ± 9.8	160 ± 70 (n = 6)	0.93 ± 0.12	31 ± 7.1	330 ± 90 (n = 6)
	Gal-S ₂ βCD	1.4 ± 0.3	3.6 ± 1.0	30 ± 10 (n = 3)	1.2 ± 0.51	5.3 ± 2.8	44 ± 30 (n = 3)

^a Data from ref 27.

of Gal-S₂βCD (Table 2), indicating a difference in the size or shape of the cavity of Glc-S₂βCD (**9**) as compared to Gal-S₂βCD (**10**), as was found from the NMR and molecular dynamics studies. Amplitude histograms show only one current blockade level, which suggests that there is only one binding site for Glc-S₂βCD or Gal-S₂βCD within the lumen of the (M113N)₇ pore, as is the case for βCD itself.^{26,27} The *I*-*V* (current versus voltage) curves for (M113N)₇·Glc-S₂βCD (Figure 5B) and (M113N)₇·Gal-S₂βCD recorded in 1 M NaCl are similar to the curve for (M113N)₇·βCD.^{26,27}

The binding of Glc-S₂βCD (**9**) and Gal-S₂βCD (**10**) to the (M113F)₇ pore was also investigated. At pH 7.5 and -40 mV, the mean conductance was reduced from 653 ± 44 to 134 ± 11 pS for Glc-S₂βCD (M113F₇·Glc-S₂βCD) and from 647 ± 9 to 209 ± 2 pS for Gal-S₂βCD (M113F₇·Gal-S₂βCD) (Table 2 and Figure 6A). At +40 mV, similar blockades by Glc-S₂βCD and Gal-S₂βCD were found (Table 2). Glc-S₂βCD (**9**) shows a larger blockade of the conductance of the (M113F)₇ pore than either βCD or Gal-S₂βCD (**10**) (Table 2). The *I*-*V* curves for (M113F)₇, (M113F)₇·Glc-S₂βCD, and (M113F)₇·Gal-S₂βCD show properties similar to the corresponding curves obtained with (M113N)₇ (Figure 6B).

The rate constants, *k*_{on}, *k*_{off}, and equilibrium dissociation constants (*K*_d) were determined for the interactions of Glc-S₂βCD (**9**) and Gal-S₂βCD (**10**) with the (M113N)₇ and (M113F)₇ pores (Table 3). Exemplifying our approach, histograms displaying the dwell times for Gal-S₂βCD (**10**) in the lumen of the (M113N)₇ pore could be fitted to single exponential distributions for data obtained at -40 mV (Figure 7A and B). These data affirm that Gal-S₂βCD, like βCD, lodges at a single site in the lumen of the pore, which is accessible from the trans side of the bilayer. Therefore, the kinetics of the interaction between Gal-S₂βCD and the (M113N)₇ pore must be a simple bimolecular interaction as seen for βCD.²⁷ As expected, the plot of 1/*τ*_{on} versus [Gal-S₂βCD] was linear (Figure 7C), the slope of which yielded the association rate constant *k*_{on}. In contrast, 1/*τ*_{off} is independent of [Gal-S₂βCD] (Figure 7D). At both negative and positive trans-membrane potentials, the dwell times (32–260 ms) of Glc-S₂βCD and Gal-S₂βCD in the (M113F)₇ pore are slightly longer than the corresponding values (18–33 ms) for the (M113N)₇ pore. As compared to the dwell times (12–26 s) of βCD in the (M113N)₇ and (M113F)₇ pores,²⁷ the two new CDs have several hundred-fold shorter dwell times in these mutants, but the dwell times are much longer in the mutant

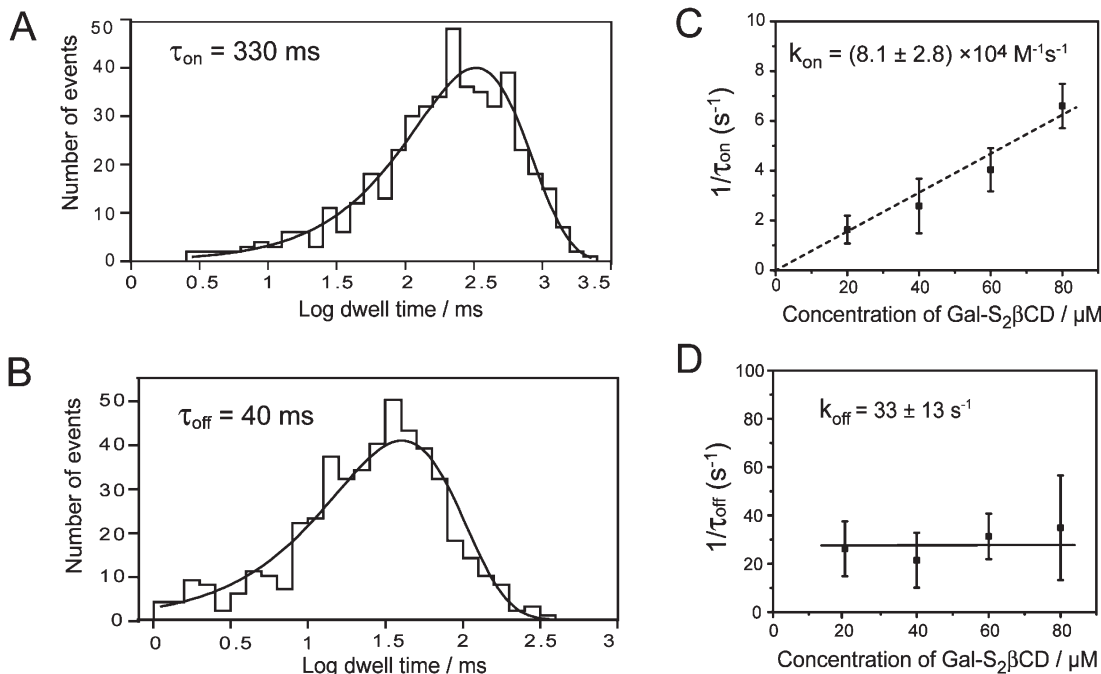


Figure 7. Kinetics of the interaction of Gal-S₂βCD (**10**) with the (M113N)₇ pore at -40 mV. (A) Histogram displaying the interevent intervals representing the unoccupied state of the (M113N)₇ pore (τ_{on}) fitted to a single-exponential distribution. (B) Histogram of the dwell times (τ_{off}) for Gal-S₂βCD (**10**) lodged within the pore. Data were from a single-channel recording made with 40 μM Gal-S₂βCD trans, in 10 mM sodium phosphate, 1 M NaCl at pH 7.5 in both chambers. (C) The rate constant k_{on} was obtained from the slope of the linear fit to $1/\tau_{\text{on}}$ versus [Gal-S₂βCD]. (D) The rate constant k_{off} is independent of [Gal-S₂βCD] and was obtained from the average of the $1/\tau_{\text{off}}$ values.

pores than that of βCD in the WT-αHL pore (<1 ms).²⁶ These results suggest potential applications of the two synthetic CDs as molecular adaptors for stochastic sensing because of their relatively long dwell times with the mutant pores.¹² Equilibrium dissociation constants ($K_d = k_{\text{off}}/k_{\text{on}}$) were calculated, and they are also about a thousand times larger than that of βCD. Because there are only minor changes in the value of k_{on} , the K_d values largely reflect k_{off} (Table 3). Those K_d values are ~10-fold lower than the dissociation rate constants for βCD from wild-type αHL.²⁶

Interactions of Glc-S₂βCD (9**) and Gal-S₂βCD (**10**) with Guest Molecules.** To evaluate the affinity of Glc-S₂βCD (**9**) and Gal-S₂βCD (**10**) with guest molecules and the potential use of these cyclic sugars as new adaptors,¹² we carried out stochastic sensing experiments. The model guest molecule 2-adamantanamine (2AD) (80 μM) was added to the buffer at pH 7.5 in the trans chamber, while either Glc-S₂βCD or Gal-S₂βCD was binding to the (M113F)₇ pore, but no clear current substates were observed when either +40 or -40 mV was applied. This indicates that 2AD, which is strongly bound by βCD (**1**) (dwell times are 0.7–1.6 ms),²⁹ is not bound by either Glc-S₂βCD or Gal-S₂βCD, at least when they are lodged within the pore.

Surprised by this dramatic retuning of the binding of a guest molecule displaying symmetry, sodium deoxycholate (DOC)^{57–59} (Figure 8A) was tested as an asymmetric guest. When DOC was introduced into the trans chamber in the presence of an (M113F)₇ pore and βCD (**1**) or Glc-S₂βCD (**9**) or Gal-S₂βCD (**10**) in 10 mM sodium phosphate, pH 7.5, 1 M NaCl, at -40 mV, clear reversible binding events were observed (Figure 8). The binding of DOC to βCD (**1**) produced a 99% current block and two types of binding events (mean dwell times, $\tau_{\text{off},1} = 0.8$ ms (type 1 event) and $\tau_{\text{off},2} = 158$ ms (type 2 event)) (Figure 8A). The interevent intervals (τ_{on}) were determined for each of the two

classes of events by using $\tau_{\text{on},1} = \tau_{\text{on}}/f_1$ and $\tau_{\text{on},2} = \tau_{\text{on}}/f_2$, where τ_{on} is the overall interevent interval (type 1 and 2 events) and f_1 and f_2 are the number of short and long events as a fraction of the total number of events, as determined from the dwell time histograms.⁶⁰ The fractions of the short events (f_1) and long events (f_2) were 0.3 ± 0.02 and 0.7 ± 0.02 of the total (Figure 8A). The k_{on} values ($k_{\text{on},1}$ and $k_{\text{on},2}$) were calculated on the basis of the equation ($k_{\text{on},1(\text{or } 2)} = 1/(\tau_{\text{on},1(\text{or } 2)} [\text{DOC}])$) (Table 4). The K_d values ($K_{d,1}$ and $K_{d,2}$) for the binding of DOC to βCD were calculated on the basis of the equation $K_{d,1(\text{or } 2)} = k_{\text{off},1(\text{or } 2)}/k_{\text{on},1(\text{or } 2)}$, where $k_{\text{off},1(\text{or } 2)} = 1/\tau_{\text{off},1(\text{or } 2)}$ (Table 4). In contrast, DOC produced only one type of binding event with either (M113F)₇·Glc-S₂βCD (Figure 8B) or (M113F)₇·Gal-S₂βCD (Figure 8C) at -40 mV. The mean dwell times of the binding events for DOC to Glc-S₂βCD and Gal-S₂βCD were 9.5 ms (Figure 8B) and 2.0 ms (Figure 8C), respectively. The respective mean interevent interval values (τ_{on}) for DOC·Glc-S₂βCD·(M113F)₇ and DOC·Gal-S₂βCD·(M113F)₇ were also obtained by fitting single exponentials to dwell time histograms, and the k_{on} and K_d values were calculated (Table 4). In all three cases, DOC also associated with the (M113F)₇ pore itself (Figure 8A–C) presumably due to direct interactions of the aromatic Phe-113 rings with DOC as found for nitroaromatics like TNT.¹⁸ The k_{off} , k_{on} , and K_d values for the direct binding of DOC to the (M113F)₇ pore were also calculated (Table 4).

■ DISCUSSION

Synthesis and Structures of Glc-S₂βCD (9**) and Gal-S₂βCD (**10**).** To expand the range of host–guest interactions including use of CDs as adaptors, one possible approach is to modify the functional groups of CDs,^{25,30,61} whereas another is the alteration

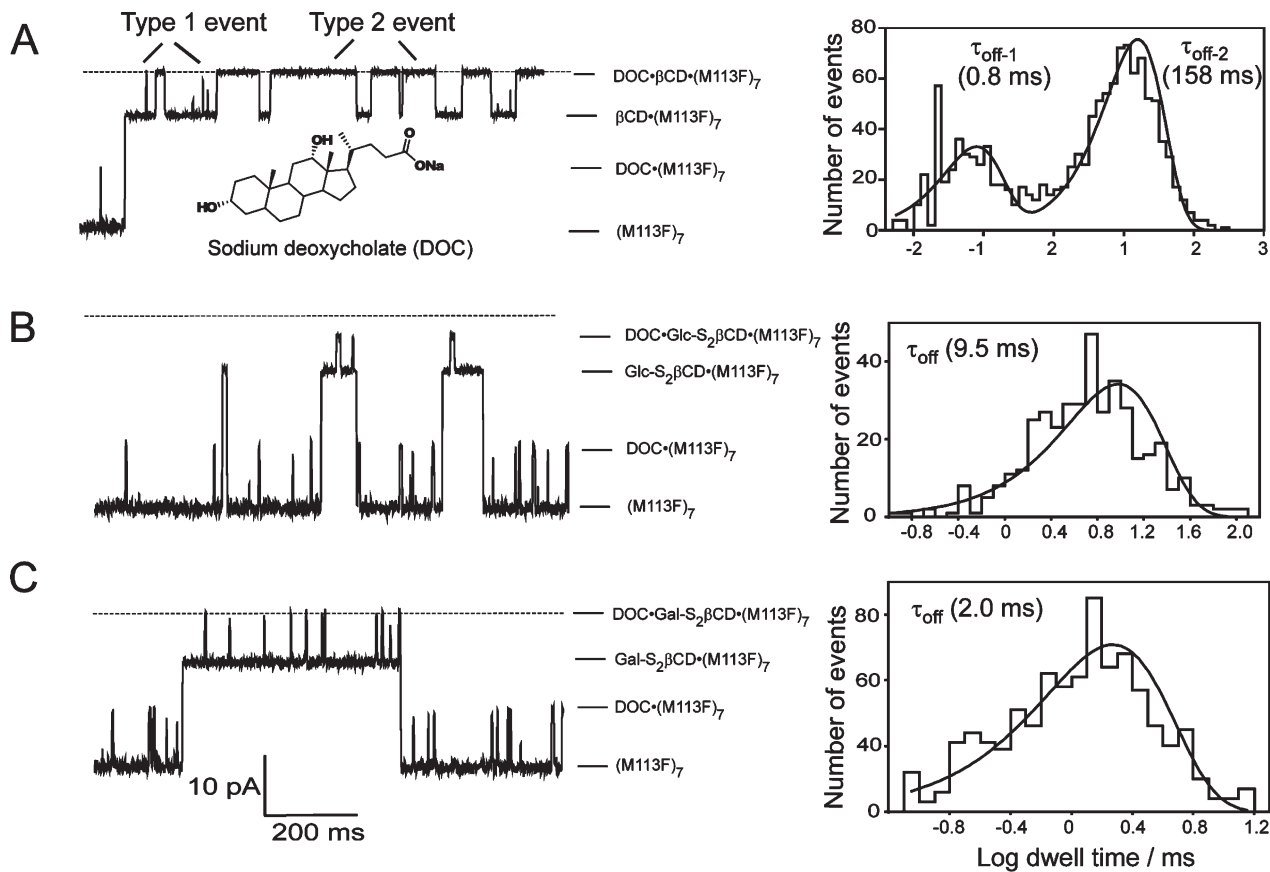


Figure 8. Comparison of the binding of DOC to β CD (**1**), Glc-S₂ β CD (**9**), and Gal-S₂ β CD (**10**) lodged within the (M113F)₇ pore. (A) Current trace from a single pore in the presence of both 30 μ M DOC (structure shown in inset) and 10 μ M β CD in 10 mM sodium phosphate, 1 M NaCl, pH 7.5, at -40 mV (left). The broken line indicates zero current. A histogram of the dwell times of DOC bound to β CD fitted to a double-exponential function (right). The mean dwell times for the short events (type 1) and the long events (type 2) are 0.8 and 158 ms, respectively. (B) Current trace from a single pore with both 30 μ M DOC and 10 μ M Glc-S₂ β CD in the trans chamber (left). A histogram of the dwell times of DOC bound to Glc-S₂ β CD fitted to a single-exponential function (right). (C) Current trace from a single pore with both 30 μ M DOC and 10 μ M Gal-S₂ β CD in the trans chamber (left). A histogram of the dwell times of DOC bound to Gal-S₂ β CD fitted to a single-exponential function (right).

Table 4. Comparison of Kinetic Parameters for Host–Guest Interactions between DOC and β CD (1**), Glc-S₂ β CD (**9**), and Gal-S₂ β CD (**10**) Lodged within the (M113F)₇ Pore**

kinetic parameters	DOC- β CD (event type 1)	DOC- β CD (event type 2)	DOC-Glc-S ₂ β CD (9)	DOC-Gal-S ₂ β CD (10)	DOC-(M113F) ₇
τ_{off} (ms)	0.80 ± 0.1	160 ± 9	9.0 ± 1.5	1.9 ± 0.6	3.4 ± 0.3
k_{off} (s ⁻¹)	1300 ± 160	6.1 ± 0.34	110 ± 19	540 ± 170	290 ± 26
k_{on} (M ⁻¹ s ⁻¹) $/10^5$	3.9 ± 0.6	8.9 ± 1.1	16 ± 5.0	15 ± 1.5	15 ± 5.0
K_d (M) $\times 10^4$	33 ± 7.3 ($n = 4$)	0.067 ± 0.009 ($n = 4$)	0.69 ± 0.03 ($n = 4$)	3.6 ± 1.2 ($n = 6$)	1.9 ± 0.73 ($n = 6$)

of the skeleton and hence the cavity of CDs. As compared to substituent-functionalized CDs, relatively few skeleton-modified CDs have been synthesized,^{31–38} primarily because of the associated synthetic challenge. To incorporate disulfide bonds into β CD (**1**), it was essential to produce a dithioheptasaccharide that was readily cyclized by oxidation. The spontaneous formation of a disulfide bond in both Glc-S₂ β CD (**9**) and Gal-S₂ β CD (**10**) in the Zemplén deacetylation step may have been aided by the proximity of the two thiols of the intermediate dithiosugars. Indeed, linear maltohexasaccharide and maltoheptasaccharide have been shown to adopt coiled conformations in solution and the solid state,^{62,63} which might favor the formation of cyclic structures through preorganization.⁶⁴

The combined NMR and molecular dynamics studies indicate that conformational differences relative to β CD exist in both **9**

and **10**, and these differences are localized around the disulfide bridges (Figure 4). The sugar residues in the remaining rings C, D, E, and F of the macrocycles adopt conformations that are very similar to those observed for β CD. The disulfide bond in **9** also resulted in a slow dynamic interchange between conformers **9a** and **9b** (Figure 4B and C) involving primarily rings A, B, and G as indicated by significant resonance broadening in the proton spectrum (Figure S5). No such dynamic broadening was observed for **10**, possibly due to a more rigid cyclic structure that restricted conformational flexibility in contrast to the more elliptical and evidently more dynamic structure of **9**.

Comparison of Gal-S₂ β CD (**10**) with β CD indicates a large difference in conformation of rings A and B whereby the disulfide bond-induced strain in the macrocycle is relieved by a dramatic

flipping of ring A to a trans orientation. Such “flipped” arrangements are also found in larger CDs.^{46–48} The dihedral angles of C1–S–S–C4' in the conformers **9a** and **9b** of Glc-S₂βCD and Gal-S₂βCD (**10**) are found to be −97.2°, −99.4°, and −81.2°, respectively, which are close to ±90° often found in disulfide bonds in protein structures.⁶⁵ Both the insertion of a disulfide linkage and the change of configuration induce a large conformational change in the macrocycles, thereby influencing both the shape and the cavity environment of the resulting synthetic CDs through the formation of asymmetrically placed “bulges” (Scheme 1A, Figure 4).

Interaction of Glc-S₂βCD (9**) and Gal-S₂βCD (**10**) with Protein Pores.** The interaction of carbohydrates with proteins is an area of intense study.^{66–68} The interactions of βCD (**1**) and proteins have previously revealed a number of different binding modes such as hydrogen-bonding and C–H···π interactions.^{28,67} Moreover, studies on the interactions of βCD and engineered protein pores have been examined through single-channel recording.^{26–28} Here, we studied the binding of disulfide-engineered CDs with the (M113N)₇ and (M113F)₇ pores, because these mutant pores bind βCD ~10⁴ times more tightly than the wild type,²⁷ and the crystal structures of the mutants with βCD bound have been determined.²⁸

Strikingly, both disulfide CDs showed decreased binding affinities (Table 3), with K_d about a thousand times larger than that of βCD with the (M113N)₇ and (M113F)₇ pores.^{26,27} The different binding properties (Table 2) and kinetic constants (Table 3) of Glc-S₂βCD (**9**) and Gal-S₂βCD (**10**) with respect to the (M113N)₇ and (M113F)₇ pores suggest that they bind at the M113 site, as does βCD.^{23,26,27} To better understand their binding mechanisms, models of the binding sites for the rigid Gal-S₂βCD (**10**) with the (M113N)₇ and (M113F)₇ pores and the crystal structures of βCD with the mutant pores were compared (Figure 9). They suggest that portions of the hydrogen-bonding network between the seven M113N residues and βCD²⁸ are disrupted when the βCD is replaced by the irregularly shaped Gal-S₂βCD (**10**). The mean distance from the amide oxygen atom in the side chain of Asn-113 to that of the 2-hydroxy group of βCD is $2.69 \pm 0.14 \text{ \AA}$ ($n = 7$). However, this distance is increased to 3.83 \AA for ring B and 3.25 \AA for ring G in the binding of Gal-S₂βCD, and hydrogen bonding to the distorted ring A is also lost (Figure 9A). Unlike the crystal structure of the (M113N)₇·βCD complex in which the secondary hydroxyls of βCD face the cis side of the pore, the (M113F)₇ pore requires the primary hydroxyls of βCD to be oriented in this direction. In the crystal structure of the (M113F)₇·βCD complex, the seven resulting cooperative C–H···π interactions are seen to stabilize the complex.^{28,69} The mean distance from the center of the phenyl ring of Phe-113 to the C-6 atom of βCD is $4.64 \pm 0.25 \text{ \AA}$ ($n = 7$), slightly larger than C–H···π distances (3.5–4.5 Å) typically found in proteins.⁷⁰ However, this distance is increased to 5.33 \AA for C-6G of Gal-S₂βCD, and the interaction is lost entirely for the altered ring A of Gal-S₂βCD (Figure 9B). This therefore suggests that the irregular shape of Gal-S₂βCD strongly disrupts the C–H···π interactions. Reduced binding of Glc-S₂βCD to the αHL mutants (Table 3) is also likely attributable to the distorted asymmetric conformations (Figure 4B and C).

Interestingly, the range ($K_d = (1.8\text{--}9.8) \times 10^{-4} \text{ M}$) (Table 3) of the binding constants for the two asymmetric CDs with symmetric (M113N)₇ or (M113F)₇ pores is comparable to that ($K_d = (0.1\text{--}10) \times 10^{-4} \text{ M}$) of βCD to the two asymmetric

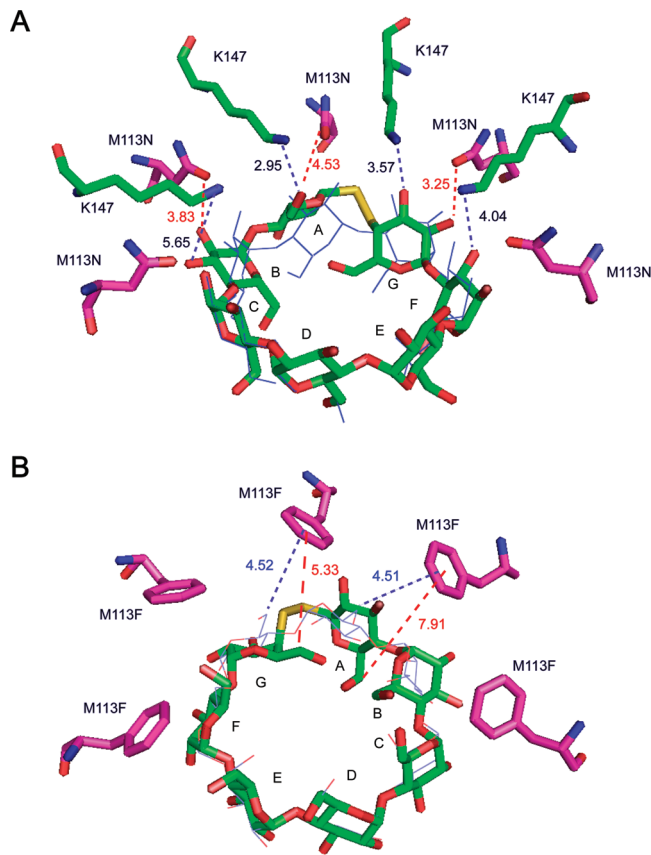


Figure 9. Superposition of the NMR structure of Gal-S₂βCD (**10**) on the crystal structures of (M113N)₇·βCD (PDB code 3M4E) and (M113F)₇·βCD (PDB code 3M3R). (A) Side chains of five Asn-113 and four Lys-147 of the (M113N)₇ pore are shown as stick models (the other two Asn and three Lys are not shown for a better view). βCD is shown as a skeletal model (blue). Gal-S₂βCD is shown as a stick model (oxygen, red; carbon, green; sulfur, yellow). The mean distances for the hydrogen bonding of the oxygen atoms of the side chain of the Asn-113 residues with the 2-hydroxyl groups of βCD and the nitrogen atoms of Lys-147 residues with the 3-hydroxyl groups of βCD are $2.69 \pm 0.14 \text{ \AA}$ ($n = 7$) and $3.34 \pm 0.20 \text{ \AA}$ ($n = 7$), respectively. The distance of the oxygen atom of the side chain of Asn-113 to the hydroxyl group of ring B of Gal-S₂βCD is increased to 3.83 \AA , indicating no hydrogen bonding between them. The distance of the ε-nitrogen atom in the nearest Lys-147 to the 3-hydroxyl group of ring B in **10** is also increased dramatically, resulting in the loss of hydrogen bonding as well. (B) Side chains of only five Phe-113 residues of the (M113F)₇ pore are shown as stick models (pink). Two molecules of βCD were found in the crystal structure of (M113F)₇·βCD. Here, only the βCD molecule that directly interacts with the Phe-113 side chains is shown as a skeletal model (blue) and compared to Gal-S₂βCD (**10**). The loss of C–H···π interactions between Gal-S₂βCD with the (M113F)₇ pore occurs due to the distorted structure.

heteroheptamers, (M113N)₅(WT)₂ and (M113F)₅(WT)₂.²⁸ The combined C_7 symmetry of both βCD and αHL is clearly essential for their tight mutual interaction; mismatching is created by loss of symmetry in either the pores ((M113N)₅(WT)₂ and (M113F)₅(WT)₂) or the CDs (Gal-S₂βCD and Glc-S₂βCD).

Interaction of Glc-S₂βCD (9**) and Gal-S₂βCD (**10**) with Guest Molecules.** The alteration of the cavity of symmetric βCD (**1**) to the asymmetric Glc-S₂βCD (**9**) and Gal-S₂βCD (**10**) was investigated by studying the ability of the CDs to

recognize small molecules in stochastic sensing. Strikingly, 2AD, a molecule with symmetry, with strong binding to C_7 -symmetric β CD ($K_d = (1.0 \pm 0.2) \times 10^{-4}$ M),²³ hardly bound to either asymmetric Glc-S₂ β CD or Gal-S₂ β CD. The asymmetric and stronger binding compound (DOC)^{57–59} was also examined by single-channel recording. The two different dissociation constants found for the binding of DOC to β CD ($K_{d,1} = (6.7 \pm 0.9) \times 10^{-6}$ M and $K_{d,2} = (3.3 \pm 0.73) \times 10^{-3}$ M) are of a similar magnitude to those found previously (1.6×10^{-6} ; 1.4×10^{-3} M) from NMR studies.^{57,59} The two different binding modes probably arise because the head and tail groups of DOC can bind β CD differently.⁵⁷ The K_d values for DOC to Glc-S₂ β CD and Gal-S₂ β CD are smaller than those for one of the binding modes ($K_{d,1}$) for DOC to β CD but larger than for the other mode ($K_{d,2}$) of β CD. The K_d of DOC for Glc-S₂ β CD is smaller than that for Gal-S₂ β CD, again indicating differences in the asymmetric cavities of these two stereoisomers (**9** and **10**). Thus, skeleton engineering of β CD has finely modulated the binding selectivity of guest molecules. Further screening of a large number of “guests” with these “hosts” by single-channel recording will delineate the full binding spectrum of these synthetic asymmetric CDs.

In conclusion, we have tuned the cavity and overall size of β CD by replacing a single oxygen atom in the ring skeleton by a disulfide unit in two different configurations. The three-dimensional NMR structures of the two stereoisomeric CDs show distorted conformations as compared to natural β CD. Both skeleton-modified CDs are useful probes for the α HL protein pore structures. They also showed altered selectivity for guest molecules when bound to mutant pores as adaptors. The asymmetric tuning of the CD cavity within the pore provides a new strategy for stochastic sensing that can alter relative selectivities toward asymmetric versus symmetric molecules.

MATERIALS AND METHODS

Chemical Synthesis of Glc-S₂ β CD (9) and Gal-S₂ β CD (10). 2,3-Di-O-acetyl-4,6-O-benzylidene- α -D-glucopyranosyl-[$(1 \rightarrow 4)$ -2,3,6-tri-O-acetyl- α -D-glucopyranosyl]₅-($1 \rightarrow 4$)-1,2,3,6-tetra-O-acetyl- α , β -D-glucopyranose (**3**). A mixture of maltoheptasaccharide **2** (0.5 g, 0.43 mmol), α , α -dimethoxytoluene (135 μ L, 0.86 mmol, 2 equiv), and p-toluenesulfonic acid monohydrate (12 mg) in dry *N,N*-dimethylformamide (5 mL) was initially rotated for 6 h in a rotary evaporator at 50 °C and then stirred for another 10 h. After the reaction mixture was cooled, the acid was neutralized with triethylamine (50 μ L), and the solvent was evaporated. Without further purification, dry pyridine (5 mL) and acetic anhydride (3 mL) were added, and the solution was heated at 80 °C for 2 h. After evaporation of the solvent, the residue was partitioned between DCM (10 mL) and water (10 mL), and the aqueous layer was re-extracted with DCM (3 \times 10 mL). The combined organic layers were washed with saturated NaHCO₃ (150 mL) until pH 7 was obtained, brine (20 mL), dried over MgSO₄, filtered, and concentrated in vacuo. The product was purified by silica gel chromatography eluting with toluene: EtOAc (1:1–1:2) to afford 2,3-di-O-acetyl-4,6-O-benzylidene- α -D-glucopyranosyl-[$(1 \rightarrow 4)$ -2,3,6-tri-O-acetyl- α -D-glucopyranosyl]₅-($1 \rightarrow 4$)-1,2,3,6-tetra-O-acetyl- α , β -D-glucopyranose (0.2 g, total yield: 22%) as a white foam; $[\alpha]^{22}_D + 123.3$ (*c* 0.8 in CHCl₃). IR ν_{max} (film): 2960, 1750 (s, C=O), 1653, 1371, 1236, 1034 cm⁻¹. δ_H (400 MHz, CDCl₃, α/β 1:3) of β anomer of **3**: 1.97, 1.98, 2.00, 2.04, 2.06, 2.07, 2.10, 2.12, 2.15, 2.17, 2.18, 2.19, 2.20, 2.21, 2.23, 2.26, 2.28 (66H, 12 \times s, 21 \times OAc), 3.56 (1H, t, *J* = 9.5 Hz, H-4G), 3.64 (1H, t, *J* = 10.0 Hz, H-6G), 3.70 (1H, m, H-5G), 3.80–4.04 (12H, m), 4.10–4.33, 4.45–4.60 (12H, m), 4.65–4.75 (5H, m), 4.85 (1H, m, H-2G), 5.07 (1H,

at *J* = 9.9 Hz, H-2A), 5.32–5.48 (12H, m), 5.41 (1H, s, Ph-CH-), 5.51 (1H, at *J* = 9.5 Hz, H-3A), 5.75 (1H, d, *J* = 8.1 Hz, H-1A), 7.30–7.41 (5H, m, H-Ph). α anomer of **3**: 4.90 (1H, dd, *J* = 10.3 Hz, 3.7 Hz, H-2A), 6.24 (1H, d, *J* = 3.7 Hz, H-1A). ^{13}C NMR (100 MHz, CDCl₃) of β anomer of **3**, δ_C : 20.5, 20.8, (3 \times q, 21 \times COCH₃), 60.3, 61.9, 62.1, 62.3 (4 \times t), 63.6 (1t, C-6G), 68.9 (d, C-5G), 70.1, 70.4, 70.9, 71.6, 72.9, 73.0, 73.2, 78.7 (d, C-4G), 91.2 (d, C-1A), 95.6, 95.7, 96.2, 101.6 (d, C-Ph-CH-), 126.2, 128.3, 129.0, 136.6, 168.7, 168.9, 169.5, 169.8, 169.9, 170.1, 170.3, 170.4, 170.5, 170.6, 170.8 (11 \times s, 21 \times COCH₃). α anomer of **3**, δ_C : 88.8 (d, C-1A). *m/z* (ES⁺) 2140 [M + NH₄]⁺, 2145 [M + Na]⁺. HRMS (ESI⁺), calcd the monoisotopic peak of doubly charged ion of C₉₁H₁₁₈O₅₇Na₂ [M + 2Na]^{+/2}, 1084.3090, found 1084.3060.

2,3-Di-O-acetyl- α -D-glucopyranosyl-[$(1 \rightarrow 4)$ -2,3,6-tri-O-acetyl- α -D-glucopyranosyl]₅-($1 \rightarrow 4$)-1,2,3,6-tetra-O-acetyl- α , β -D-glucopyranose (4**).** 2,3-Di-O-acetyl-4,6-O-benzylidene- α -D-glucopyranosyl-[$(1 \rightarrow 4)$ -2,3,6-tri-O-acetyl- α -D-glucopyranosyl]₅-($1 \rightarrow 4$)-1,2,3,6-tetra-O-acetyl- α , β -D-glucopyranose (**3**, 200 mg, 94 μ mol) was dissolved in 2.5 mL of 80% HOAc (aq), and heated at 45 °C for 16 h. After evaporation of the solvent, the product was purified by HPLC to give a white solid (72 mg, yield 37%). HPLC was performed using a Varian Polaris C₁₈ column (150 \times 21.2 mm i.d., 5 μ m particle size) by using a linear gradient of 40–100% acetonitrile in water over 25 min at a flow rate of 8 mL min⁻¹ monitored at 215 nm with a photodiode-array ultraviolet detection system. R_f 14.4 min. HPLC-UV (213 nm). $[\alpha]^{22}_D + 93.0$ (*c* 1.0 in CHCl₃). IR ν_{max} (thin film): 2958, 1748 (s, C=O), 1371, 1237, 1034 cm⁻¹. δ_H (400 MHz, CDCl₃, α/β 1:3) of β anomer of **4**: 1.99, 2.01, 2.03, 2.05, 2.06, 2.07, 2.09, 2.10, 2.13, 2.15, 2.16, 2.19, 2.20, 2.21, 2.24 (66H, 15 \times s, 21 \times OAc), 3.60 (2H, m, H-4G, H-5G), 3.80 (1H, m, H-6G), 3.70–4.04 (12H, m), 4.10–4.35, 4.40–4.60 (12H, m), 4.70–4.80 (5H, m), 4.97 (1H, at *J* = 9.9 Hz, H-2A), 5.22 (1H, at *J* = 10.0 Hz, H-3G), 5.32–5.48 (12H, m), 5.52 (1H, at *J* = 9.5 Hz, H-3A), 5.75 (1H, d, *J* = 8.1 Hz, H-1A). α form: 6.25 (1H, d, *J* = 3.6 Hz, H-1A). ^{13}C NMR (100 MHz, CDCl₃): 20.5, 20.7, 20.8, 21.0 (3 \times q, 21 \times COCH₃), 60.4, 62.1, 62.3, 62.5 (4 \times t), 68.9, 69.1, 70.2, 70.4, 71.7, 72.0, 72.7, 72.9, 73.2, 91.2 (d, C-1A), 95.6, 95.7, 169.5, 169.6, 170.39, 170.43, 170.54, 170.65, 170.73, 170.85, 170.89 (9 \times s, 21 \times COCH₃). *m/z* (ES⁺) 2052 [M + NH₄]⁺, 2057 [M + Na]⁺. HRMS (ESI⁺), calcd the monoisotopic peak of doubly charged ion of C₈₄H₁₁₄O₅₇Na₂ [M + 2Na]^{+/2}, 1040.2903, found 1040.2933.

2,3,6-Tri-O-acetyl- α -D-glucopyranosyl-[$(1 \rightarrow 4)$ -2,3,6-tri-O-acetyl- α -D-glucopyranosyl]₅-($1 \rightarrow 4$)-1,2,3,6-tetra-O-acetyl- α , β -D-glucopyranose (5**).** 2,3-Di-O-acetyl- α -D-glucopyranosyl-[$(1 \rightarrow 4)$ -2,3,6-tri-O-acetyl- α -D-glucopyranosyl]₅-($1 \rightarrow 4$)-1,2,3,6-tetra-O-acetyl- α , β -D-glucopyranose (**4**, 70 mg, 34 μ mol) was dissolved in dry DCM, and then 1-acetoxybenzotriazole (6.5 mg, 1.1 equiv) and triethylamine (3.8 μ L) were added. The mixture was stirred at room temperature for 17 h, and the solvent was finally evaporated. HPLC purification gave a solid of **5** (52 mg, yield: 74%). R_f 15.7 min. HPLC-UV (λ_{max} = 211 nm). $[\alpha]^{22}_D + 125.7$ (*c* 0.5 in CHCl₃). IR: ν_{max} (thin film) 2960, 1748 (s, C=O), 1371, 1237, 1034 cm⁻¹. δ_H (400 MHz, CDCl₃, α/β = 1:3) of β anomer of **5**: 1.99, 2.00, 2.01, 2.02, 2.13, 2.18, 2.19, 2.23, 2.29 (66H, 10 \times s, 21 \times OAc), 3.54 (1H, t, *J* = 9.7 Hz, H-4G), 3.78 (1H, d, *J* = 9.8 Hz), 3.80–4.10 (12H, m), 4.10–4.40, 4.40–4.60 (12H, m), 4.70–4.75 (5H, m), 4.78 (1H, dd, *J*_{1,2} = 3.9 Hz, *J*_{2,3} = 9.5 Hz, H-2G), 4.96 (1H, at *J* = 9.9 Hz, H-2A), 5.22 (1H, at *J* = 10.0 Hz, H-3G), 5.32–5.48 (12H, m), 5.52 (1H, at *J* = 9.5 Hz, H-3A), 5.75 (1H, d, *J* = 8.1 Hz, H-1A). α anomer of **5**: 6.24 (1H, d, *J* = 3.7 Hz, H-1A). ^{13}C NMR (125 MHz, CDCl₃): 20.53, 20.57, 20.63, 20.77, 20.82, 20.84, 20.88, 21.01, 21.42 (3 \times q, 21 \times COCH₃), 62.25, 62.35, 62.54, 68.78, 68.89, 68.93, 68.96, 69.05, 69.07, 69.94, 70.33, 70.43, 70.48, 70.99, 71.11, 71.54, 71.64, 71.68, 71.78, 71.83, 72.30, 72.96, 73.05, 73.15, 73.25, 73.28, 73.38, 75.16, 76.75, 91.23 (d, C-1A), 95.59, 95.69, 95.78, 95.83, 169.44, 169.49, 169.54, 169.85, 170.35, 170.39, 170.44, 170.48, 170.53, 170.64, 170.65, 170.71, 170.84, 171.12, 171.39 (15 \times s, 21 \times COCH₃).

α -anomer of **5**: 87.5 (d, C-1A). m/z (ES $^+$) 2094 [M + NH $_4$] $^+$, 2099 [M + Na] $^+$. HRMS (ESI $^+$), calcd the monoisotopic peak of doubly charged ion of C₈₆H₁₁₆O₅₈Na₂ [M + 2Na] $^{+2}$ /2, 1061.2956, found 1061.2960. As an alternative method, peracetyl- β -cyclodextrin (4.9 g, 2.4 mmol) was dissolved in a mixture of acetic acid (25 mL), acetic anhydride (820 μ L), concentrated H₂SO₄ (100 μ L), and H₂O (400 μ L). After being heated at 120 °C for 10 min, the mixture cooled and was poured into cold water and extracted with EtOAc, and then the organic fraction was washed with saturated NaHCO₃ and water, dried with MgSO₄, and evaporated. Purification with repeated silica gel chromatography eluting with toluene/EtOAc gave a white solid of **5** (5 mg, 0.1%).

2,3,6-Tri-O-acetyl- α -D-galcopyranosyl-[$(1\rightarrow 4)$ -2,3,6-tri-O-acetyl- α -D-glucopyranosyl]₅-($1\rightarrow 4$)-1,2,3,6-tetra-O-acetyl- α , β -D-glucopyranose (6). 2,3,6-Tri-O-acetyl- α -D-glucopyranosyl-[$(1\rightarrow 4)$ -2,3,6-tri-O-acetyl- α -D-glucopyranosyl]₅-($1\rightarrow 4$)-1,2,3,6-tetra-O-acetyl- α , β -D-glucopyranose (**5**, 90 mg, 41.4 μ mol) was dissolved in dry DCM (2.0 mL) and pyridine (60 μ L) with stirring under N₂ and was cooled to -10 °C. Trifluoromethanesulfonic anhydride (70 μ L, 0.42 mmol, 10 equiv) was added dropwise, and the mixture was stirred for 2.5 h. After dilution with DCM (8 mL), the organic phase was washed sequentially with 10 mM HCl, saturated sodium bicarbonate solution, and water, dried over MgSO₄, filtered, and concentrated. Without purification, the crude product was dissolved in dry DMF (1 mL), NaNO₂ (15 mg) was added, and the mixture was heated at 50 °C for 2 h. DMF was evaporated, and the product was purified by HPLC to give 45 mg (yield: 50%). Rt 15.7 min. HPLC-UV (λ_{max} = 211 nm). $[\alpha]^{22}_D$ +56.9 (c 0.1 in CHCl₃). IR ν_{max} (thin film): 2923, 1747 (s, C=O), 1371, 1237, 1034 cm $^{-1}$. δ_H (500 MHz, CDCl₃, α/β 1:3) of β form of **6**: 1.99, 2.01, 2.02, 2.03, 2.04, 2.07, 2.10, 2.11, 2.14, 2.19, 2.20, 2.21, 2.22, 2.24 (66H, 11s, 21 \times OAc), 3.87–4.10 (12H, m), 4.10, 4.10–4.40, 4.40–4.60 (12H, m), 4.71–4.77 (5H, m), 4.98 (1H, t, H-2A), 5.25 (1H, dd, J = 11.4, 4.1 Hz, H-2G), 5.18 (1H, dd, J = 11.0, 2.8 Hz, H-3G), 5.32–5.48 (12H, m), 5.52 (1H, at, J = 9.1 Hz, H-3A), 5.75 (1H, d, J = 8.1 Hz, H-1A). α -form of **6**: 4.97 (1H, dd, J = 9.7, 3.5 Hz, H-2A), 6.25 (1H, d, J = 3.8 Hz, H-1A). ¹³C NMR (125 MHz, CDCl₃): 20.54, 20.73, 20.84 (3 \times q, 21 \times COCH₃), 61.9, 66.7 (C-4G), 68.6, 69.4, 69.6, 71.1, 71.5, 72.6, 72.9, 95.6, 96.3, 169.86, 170.42, 170.71, 170.84, 171.12, 171.39 (15 \times s, 21 \times COCH₃). m/z (ES $^+$) 2094 [M + NH $_4$] $^+$, 2099 [M + Na] $^+$. HRMS (ESI $^+$), calcd the monoisotopic peak of doubly charged ion of C₈₆H₁₁₆O₅₈Na₂ [M + 2Na] $^{+2}$ /2, 1061.2956, found 1061.2986.

2,3,6-Tri-O-acetyl-4-S-acetyl-4-thio- α -D-galactopyranosyl-[$(1\rightarrow 4)$ -2,3,6-tri-O-acetyl- α -D-glucopyranosyl]₅-($1\rightarrow 4$)-1-S-acetyl-2,3,6-tri-O-acetyl- β -D-glucopyranoside (7). 2,3,6-Tri-O-acetyl- α -D-glucopyranosyl-[$(1\rightarrow 4)$ -2,3,6-tri-O-acetyl- α -D-glucopyranosyl]₅-($1\rightarrow 4$)-1,2,3,6-tetra-O-acetyl- α (β)-D-glucopyranoside (**5**, 50 mg, 24 μ mol) was dissolved in dry DCM (1.0 mL) and pyridine (20 μ L) with stirring under N₂ and was cooled to -10 °C. Trifluoromethanesulfonic anhydride (35 μ L, 0.21 mmol, 8.8 equiv) was added dropwise, and the mixture was stirred for 2 h, then diluted with DCM (8 mL), washed successively with 0.1 M HCl, saturated sodium bicarbonate solution, and water, then dried over MgSO₄, filtered, and concentrated to give 35 mg, m/z (ES $^+$), 2231 [M + Na] $^+$. Without purification, the crude product was dissolved in 33% HBr in HOAc at 0 °C for 1 h and kept for 2 h at room temperature. The product was extracted by adding EtOAc (10 mL), washed successively with water, saturated sodium bicarbonate solution, and water, then dried over MgSO₄, filtered, and concentrated to give 34 mg of crude product, m/z (ES $^+$), 2251 [M + Na] $^+$. This material was dissolved in dry DMF (0.8 mL), and potassium thioacetate (8.0 mg, 4 equiv) was added. The solution was stirred overnight, then diluted with ethyl acetate, washed with water, saturated sodium bicarbonate solution, and water, dried with MgSO₄, and concentrated. The final product was purified by semipreparative HPLC to give 10 mg of **7** (overall yield: 19%). Rt 19.2 min. HPLC-UV (λ_{max} = 227 nm), $[\alpha]^{22}_D$ +33.0 (c 0.5 in CHCl₃). IR ν_{max} (thin film): 2962, 2920, 1747 (s, O=C–O, oxygen ester), 1710 (s, O=C–S, thioester), 1370, 1230, 1033 cm $^{-1}$. δ_H (500 MHz, CDCl₃) of **7**: 1.99, 2.00, 2.02, 2.03, 2.06, 2.08, 2.09, 2.11, 2.14,

2.16, 2.21, 2.21 (66H, 12s, 21 \times OAc), 2.38, 2.39 (6H, 2s, 2 \times SAC), 3.80–4.05 (12H, m), 4.10–4.40, 4.40–4.60 (12H, m), 4.36 (1H, t, J = 3.6 Hz, H-4G), 4.70–4.75 (SH, m), 4.94 (1H, dd, J = 11.0, 4.2 Hz, H-2G), 4.98 (1H, dd, J = 10.3, 9.0 Hz, H-2A), 5.29 (1H, d, J = 8.7 Hz, H-1A), 5.32–5.48 (12H, m). ¹³C NMR (125 MHz, CDCl₃): 20.54, 20.60, 20.65, 20.72, 20.86 (5 \times q, 21 \times COCH₃), 30.75, 30.80 (2 \times q, 2 \times SCOCH₃), 46.63 (d, C-4G), 62.28, 63.05, 67.09, 67.68, 68.62, 68.93, 69.07, 69.89, 70.30, 70.49, 71.47, 71.55, 71.67, 71.73, 72.33, 73.09, 73.46, 79.74 (d, C-1A), 95.56, 95.70, 95.76, 96.08, 169.45, 169.59, 169.65, 169.91, 170.40, 170.50, 170.44, 170.68, 170.74 (9 \times s, 21 \times COCH₃), 191.79 (1s, C(1A)-SCOCH₃), 193.14 (1s, C(4G)-SCOCH₃). m/z (ES $^+$), 2173 [M + Na] $^+$. HRMS (ESI $^+$), calcd for the monoisotopic peak of doubly charged ion of C₈₈H₁₁₈O₅₇S₂Na₂ [M + 2Na] $^{+2}$ /2, 1098.2780, found 1098.2776.

2,3,6-Tri-O-acetyl-4-S-acetyl-4-thio- α -D-glucopyranosyl-[$(1\rightarrow 4)$ -2,3,6-tri-O-acetyl- α -D-glucopyranosyl]₅-($1\rightarrow 4$)-1-S-acetyl-2,3,6-tri-O-acetyl- β -D-glucopyranoside (8). 2,3,6-Tri-O-acetyl- α -D-galactopyranosyl-[$(1\rightarrow 4)$ -2,3,6-tri-O-acetyl- α -D-glucopyranosyl]₅-($1\rightarrow 4$)-1,2,3,6-tetra-O-acetyl- α (β)-D-glucopyranoside (**6**, 45 mg, 21 μ mol) was used to prepare compound **8** (8 mg, yield: 18%) by a procedure similar to that for compound **7**. Rt 19.2 min. HPLC-UV (λ_{max} = 227 nm). $[\alpha]^{22}_D$ +8.2° (c 0.1 in CHCl₃). IR ν_{max} (thin film): 2923, 1747 (s, O=C–O, oxygen ester), 1710 (s, O=C–S, thioester), 1371 cm $^{-1}$. δ_H (500 MHz, CDCl₃) of **8**: 1.98, 1.99, 2.00, 2.01, 2.03, 2.05, 2.12, 2.14, 2.18, 2.19, 2.21 (66H, 12 \times s, 21 \times OAc), 2.32, 2.38 (6H, 2 \times s, 2 \times SAC), 3.73 (1H, t, J = 11.4 Hz), 3.80–4.05 (12H, m), 4.10–4.40, 4.40–4.60 (12H, m), 4.36 (1H, t, J = 3.6 Hz, H-4G), 4.70–4.75 (5H, m), 4.87 (1H, dd, J = 10.1, 3.8 Hz, H-2G), 4.98 (1H, dd, J = 10.1, 9.1 Hz, H-2A), 5.35 (1H, d, J = 8.5 Hz, H-1A), 5.32–5.46 (12H, m). ¹³C NMR (125 MHz, CDCl₃): 20.63, 20.56, 20.74, 20.86 (5 \times q, 21 \times COCH₃), 30.58, 30.80 (2 \times q, 2 \times SCOCH₃), 43.60 (d, C-4G), 62.3, 62.06, 62.69, 62.77, 67.09, 67.40, 68.90, 69.1, 69.5, 69.90, 70.40, 70.50, 71.60, 71.70, 71.70, 72.20, 73.1, 73.20, 73.37, 73.45, 79.74 (d, C-1A), 95.60, 95.68, 95.76, 95.87, 169.42, 169.50, 169.56, 169.65, 169.90, 170.34, 170.38, 170.68, 170.74 (9s, 21 \times COCH₃), 191.8 (1s, C(1A)-SCOCH₃), 192.5 (1s, C(4G)-SCOCH₃). m/z (ES $^+$), 2173 [M + Na] $^+$. HRMS (ESI $^+$), calcd for the double charged monoisotopic peak of C₈₈H₁₁₈O₅₇S₂Na₂ [M + 2Na] $^{+2}$ /2, 1098.2780, found 1098.2800.

Cyclo-S-S-(4-thio- α -D-glucopyranosyl)₅-($1\rightarrow 4$)-1-thio- β -D-glucopyranosyl Disulfide (9) (Glc-S₂BCD). 2,3,6-Tri-O-acetyl-4-S-acetyl- α -D-glucopyranosyl-[$(1\rightarrow 4)$ -2,3,6-tri-O-acetyl- α -D-glucopyranosyl]₅-($1\rightarrow 4$)-1-S-acetyl-2,3,6-tri-O-acetyl- β -D-glucopyranoside (**8**, 8.0 mg, 3.7 μ mol) and 0.1 mL of NaOMe in 10 mg/mL (1 mg, 18.5 μ mol, 4.7 equiv) were added to a stirred solution of MeOH (5 mL). After 12 h, ESI-MS analysis showed the complete reaction and the formation of oxidized products. The reaction was neutralized with the addition of Dowex-50 H $^+$ ion-exchange resin after which point the reaction was filtered and concentrated in vacuo. Further HPLC purification with a Lichrosphere amino column (250 \times 4.60 mm i.d., particle size 5 μ m) (Supelco Inc.) eluting with CH₃CN/water (6:4) and detecting with a refractive index detector gave compound **9** as a white powder (0.4 mg, yield 12%). $[\alpha]^{22}_D$ +202.1 (c 0.02 in H₂O). IR ν_{max} (KBr): 3421, 2923, 1636, 1031, 577 cm $^{-1}$. ¹H and ¹³C NMR (D₂O) of **9** at 322 K: see Tables S1 and S2. ¹H NMR (700 MHz, D₂O) of **9** at 292 K (with HOD at 4.70 ppm), δ_H : 5.47 ppm (2H, brs, H-1B and 1G), 5.11 (1H, d, J = 3.3 Hz, H-1C), 4.98 (1H, d, J = 3.3 Hz, H-1F), 4.92 (1H, d, J = 4.1 Hz, H-1E), 4.91 (1H, J = 3.6 Hz, H-1D), 4.34 (1H, d, J = 9.3 Hz, H-1A), 3.97 (1H, d, J = 10.0 Hz, H-3G), 3.42–3.90, 3.32 (1H, brs, H-2A), and 2.51 (1H, d, J = 10.4 Hz, H-4G). m/z (ES $^+$), 1205.3 [M + Na] $^+$; m/z (ES $^-$), 1181.3 [M – H] $^-$. HRMS (ESI $^+$), calcd for the monoisotopic peak of C₄₂H₇₀O₃₄S₂Na [M + Na] $^+$ 1205.3082, found 1205.3039.

Cyclo-S-S-(4-thio- α -D-galactopyranosyl)₅-($1\rightarrow 4$)-1-thio- β -D-glucopyranosyl Disulfide (10) (Gal-S₂BCD). 2,3,6-Tri-O-acetyl-4-S-acetyl- α -D-galactopyranosyl-[$(1\rightarrow 4)$ -2,3,

6-tri-O-acetyl- α -D-glucopyranosyl]₅-(1 \rightarrow 4)-1-S-acetyl-2,3,6-tri-O-acetyl- β -D-glucopyranoside (7, 8.5 mg, 3.9 μ mol) and 0.1 mL of NaOMe in 10 mg/mL (1 mg, 18.5 μ mol, 4.7 equiv) were added to a stirred solution of MeOH (3 mL). ESI-MS of the reaction product indicated completion of the reaction. The reaction solution was neutralized with the addition of Dowex-50 H⁺ ion-exchange resin after which point the reaction was filtered and concentrated in vacuo. Further HPLC purification with a Lichrosphere amino column eluting with CH₃CN/water (6:4) and detecting with a refractive index detector gave compound **10** as a white powder (0.5 mg, yield 11%). $[\alpha]^{22}_D +127.1$ (*c* 0.1 in H₂O). IR ν_{max} (KBr): 3404, 2928, 1636, 1029, 579 cm⁻¹. ¹H and ¹³C NMR (D₂O) of **10** at 292 K; see Tables S1 and S2. *m/z* (ES⁺), 1205 [M + Na]⁺. HRMS (ESI⁺), calcd for the monoisotopic peak of C₄₂H₇₀O₃₄S₂Na [M + Na]⁺ 1205.3082, found 1205.3058.

NMR Structural Characterization of Glc-S₂ β CD (9) and Gal-S₂ β CD (10). NMR analyses were performed on a Bruker AVIII NMR spectrometer operating at 700 MHz (¹H) and equipped with a ¹H {¹³C, ¹⁵N} TCI cryoprobe. Samples were prepared from ~200 μ g of CDs in 75 μ L of D₂O and placed in 2 mm NMR tubes. Chemical shifts are referenced to external TSP at 0.00 ppm recorded at the same temperature as the CD samples. NMR assignments were obtained initially from analysis of 2D COSY, multiplicity-edited HSQC, and TOCSY data sets using solvent presaturation where necessary. In the case of Gal-S₂ β CD (10), additional 1D selective TOCSY and NOESY experiments were also employed to isolate the spin systems for each sugar ring. These experiments employed single PFG spin-echoes with 80 ms Gaussian pulses for selective excitation of the anomeric protons. The 1D TOCSY experiments used DIPSI-2 isotropic mixing with incorporation of zero-quantum suppression scheme⁷¹ and mixing times of up to 250 ms, while 1D NOESY used mixing times of 500 ms. Sugar sequence assignments were derived from intra-ring H1–H4 NOEs, and interproton distances (from the anomeric protons) were estimated from relative intensities in the 1D NOESY spectra using the intra-ring H1–H2 NOEs as internal reference (2.45 Å). The ¹J_{CH} coupling constants were measured from F₂ traces extracted from a high-resolution ¹³C-coupled HSQC experiment. The measurement of ³J_{CH} coupling constants was performed by fitting of phase-sensitive HMBC multiplet structures according to the method of Keeler.⁷² Thus, the H1–C4 crosspeak fine structures were used for the measurements via fitting to reference multiplets extracted from a suitable 1D ¹H spectrum. The H1B–C4A crosspeak was too weak to derive a reliable fit, but the coupling was estimated to be somewhat below 2 Hz by comparison with data extracted for other peaks in the HMBC data set.

For Glc-S₂ β CD (9), assignments were derived at 322 K to afford sharper resonances arising from faster conformational exchange. Because of the reduced correlation times, 2D ROESY spectra were used to determine NOEs and made use of an alternating-phase spin-lock of 400 ms to suppress TOCSY-derived transfers.⁷³ Where possible, estimates of internuclear distances were made from volume integration of 2D cross-peaks.

Molecular Dynamics Simulations. Molecular modeling was performed on a Silicon Graphics Fuel workstation using Insight II and Discover software (Accelrys Inc.). Restrained molecular dynamics simulations were performed in vacuo with a dielectric constant of eighty using the cvff force field. As no parameters were available for the exoanomeric effect for a dithio-glycosidic linkage, no extra terms were added to the standard force field for the exoanomeric effect. Starting structures and geometries were generated on the basis of the crystal structure of β CD⁵⁴ and typical glycosidic torsion angles,⁵⁶ and then energy minimized using a steepest descent algorithm. Simulations were typically run at 300 K for 300 ps using a 1 fs step size, and saving structures every 500 fs. Distance restraints were based on the observed interproton NOEs. In some runs, torsion angle restraints based on observed ³J_{CH} coupling constants were included. Simulations were usually performed without

restraints across the A–G linkage, but some simulations included these. Some simulations were performed at higher temperatures to increase the probability that transitions between stable conformations would be observed, and, for these, restraints to maintain the ⁴C₁ chair conformation of the saccharide rings were also included. Restraints were typically 5–10 times the thermal energy, and so the final results are heavily biased toward the experimental data. Stable conformations reported are based on the average structure adopted over a 100–200 ps time.

Planar Bilayer Recordings. Planar bilayer recordings were made at 22 \pm 2 °C. The buffer for bilayer recording contained 1 M NaCl and 10 mM dibasic sodium phosphate, in deionized water, and was titrated to pH 7.5 with aqueous HCl. The bilayer was formed from 1,2-diphytanoyl-sn-glycerophosphocholine (Avanti Polar Lipids) over an orifice 50–100 μ m in diameter.⁷⁴ The orifice had been pretreated with hexadecane in pentane, and the lipid was transferred to the chambers in pentane. The cis chamber was at ground. A positive potential indicates a higher potential in the trans chamber of the apparatus, and a positive current is one in which cations flow from the trans to the cis side. Experiments were initiated by the addition of heptameric α HL (Supporting Information) to the cis chamber, to a final concentration of 5–50 ng/mL, with stirring until a single channel appeared. β CD, Glc-S₂ β CD (9), and Gal-S₂ β CD (10) were added to the trans chamber at 5–40 μ M. The amplifier's internal low-pass Bessel filter was set at 5 kHz. Data were acquired at a sampling rate of 20 kHz.

Data Analysis. Current traces were analyzed with pClamp 10.2 software (Axon Instruments). Events were detected using the Event Detection feature and were used to construct amplitude and dwell time histograms. Clampfit 10.2 was used for curve fitting and graph presentation. τ_{on} and τ_{off} for CDs and DOC at either -40 or +40 mV were obtained from dwell-time histograms fitted to exponential functions by the Levenberg–Marquardt procedure. The data were plotted in logarithmic form for display. Kinetic constants for the binding of CDs to proteins and for the binding of DOC to CDs were calculated by using $k_{\text{off}} = 1/\tau_{\text{off}}$, $k_{\text{on}} = 1/\tau_{\text{on}}$ [CDs or DOC], and $K_d = k_{\text{off}}/k_{\text{on}}$, where [CDs or DOC] is the concentration of CDs or DOC. Values for unitary conductance, k_{on} and k_{off} , and K_d are quoted as the mean \pm s.d.

ASSOCIATED CONTENT

Supporting Information. Figures S1–S10. Further results, discussion, and detailed descriptions of experimental materials and methods. This material is available free of charge via the Internet at <http://pubs.acs.org>.

AUTHOR INFORMATION

Corresponding Author

ben.davis@chem.ox.ac.uk; hagan.bayley@chem.ox.ac.uk

ACKNOWLEDGMENT

We thank Mr. Robin Procter and Mr. Lingzhi Gong for the measurement of mass spectra of sugars and proteins, respectively. B.G.D. is a recipient of a Royal Society Wolfson Research Merit Award. This work was supported by an EPSRC grant to H.B. and B.G.D.

REFERENCES

- (1) Szejtli, J. *Chem. Rev.* 1998, 98, 1743–1753.
- (2) Rekharsky, M. V.; Inoue, Y. *Chem. Rev.* 1998, 98, 1875–1918.
- (3) Dodziuk, H. *Cyclodextrins and Their Complexes. Chemistry, Analytical Methods, Applications*; Wiley-VCH: New York, 2006.
- (4) Davis, M. E.; Brewster, M. *Nat. Rev. Drug Discovery* 2004, 3, 1023–1035.
- (5) Bom, A.; Bradley, M.; Cameron, K.; Clark, J. K.; van Egmond, J.; Feilden, H.; MacLean, E. J.; Muir, A. W.; Palin, R.; Rees, D. C.; Zhang, M.-Q. *Angew. Chem., Int. Ed.* 2002, 41, 265–270.

- (6) Wenz, G.; Han, B. H.; Müller, A. *Chem. Rev.* **2006**, *106*, 782–817.
 (7) Harada, A.; Hashidzume, A.; Yamaguchi, H.; Takashima, Y. *Chem. Rev.* **2009**, *109*, 5974–6023.
 (8) Chen, Y.; Liu, Y. *Chem. Soc. Rev.* **2010**, *39*, 495–505.
 (9) Kuzuya, A.; Ohnishi, T.; Wasano, T.; Nagaoka, S.; Sumaoka, J.; Ihara, T.; Jyo, A.; Komiyama, M. *Bioconjugate Chem.* **2009**, *20*, 1643–1649.
 (10) Ashcroft, B. A.; Spadola, Q.; Qamar, S.; Zhang, P.; Kada, G.; Bension, R.; Lindsay, S. *Small* **2008**, *4*, 1468–1475.
 (11) Villaonga, R.; Cao, R.; Fragoso, A. *Chem. Rev.* **2007**, *107*, 3088–3116.
 (12) Bayley, H.; Cremer, P. S. *Nature* **2001**, *413*, 226–230.
 (13) Dekker, C. *Nat. Nanotechnol.* **2007**, *2*, 209–215.
 (14) Song, L.; Hobough, M. R.; Shustak, C.; Cheley, S.; Bayley, H.; Gouaux, J. E. *Science* **1996**, *274*, 1859–1866.
 (15) Braha, O.; Walker, B.; Cheley, S.; Kasianowicz, J. J.; Song, L.; Gouaux, J. E.; Bayley, H. *Chem. Biol.* **1997**, *4*, 497–505.
 (16) Howorka, S.; Nam, J.; Bayley, H.; Kahne, D. *Angew. Chem., Int. Ed.* **2004**, *43*, 842–846.
 (17) Bayley, H. *Curr. Opin. Chem. Biol.* **2006**, *10*, 628–637.
 (18) Guan, X.; Gu, L.-Q.; Cheley, S.; Braha, O.; Bayley, H. *Chem-BioChem* **2005**, *6*, 1875–1881.
 (19) Wu, H. C.; Bayley, H. *J. Am. Chem. Soc.* **2008**, *130*, 6813–6819.
 (20) Bayley, H.; Luchian, T.; Shin, S. H.; Steffensen, M. B. In *Single Molecules and Nanotechnology*; Rigler, R., Vogel, H., Eds.; Springer: New York, 2008; pp 251–277.
 (21) Lu, S.; Li, W. W.; Rotem, D.; Mikhailova, E.; Bayley, H. *Nat. Chem.* **2010**, *2*, 921–928.
 (22) Gu, L.-Q.; Braha, O.; Conlan, S.; Cheley, S.; Bayley, H. *Nature* **1999**, *398*, 686–690.
 (23) Gu, L.-Q.; Cheley, S.; Bayley, H. *Science* **2001**, *291*, 636–640.
 (24) Kang, X. F.; Cheley, S.; Guan, X.; Bayley, H. *J. Am. Chem. Soc.* **2006**, *128*, 10684–10685.
 (25) Astier, Y.; Braha, O.; Bayley, H. *J. Am. Chem. Soc.* **2006**, *128*, 1705–1710.
 (26) Gu, L.-Q.; Bayley, H. *Biophys. J.* **2000**, *79*, 1967–1975.
 (27) Gu, L.-Q.; Cheley, S.; Bayley, H. *J. Gen. Physiol.* **2001**, *118*, 481–494.
 (28) Banerjee, A.; Mikhailova, E.; Cheley, S.; Gu, L.-Q.; Montoya, M.; Nagaoka, Y.; Gouaux, E.; Bayley, H. *Proc. Natl. Acad. Sci. U.S.A.* **2010**, *107*, 8165–8170.
 (29) Wu, H. C.; Astier, Y.; Maglia, G.; Mikhailova, E.; Bayley, H. *J. Am. Chem. Soc.* **2007**, *129*, 16142–16148.
 (30) Clarke, J.; Wu, H. C.; Jayasinghe, L.; Patel, A.; Reid, S.; Bayley, H. *Nat. Nanotechnol.* **2009**, *4*, 265–270.
 (31) Bornaghi, L.; Utile, J.-P.; Penninga, D.; Schmidt, A. K.; Dijkhuizen, L.; Schulz, G. E.; Driguez, H. *Chem. Commun.* **1996**, 2541–2542.
 (32) Morales, J. C.; Zurita, D.; Penades, S. *J. Org. Chem.* **1998**, *63*, 9212–9222.
 (33) Kida, T.; Michinobu, T.; Zhang, W.; Nakatsuji, Y.; Ikeda, I. *Chem. Commun.* **2002**, 1596–1597.
 (34) Hoffmann, B.; Bernet, B.; Vasella, A. *Helv. Chim. Acta* **2002**, *85*, 265–287.
 (35) Kikuzawa, A.; Kida, T.; Nakatsuji, Y.; Akashi, M. *J. Org. Chem.* **2005**, *70*, 1253–1261.
 (36) Bodine, K. D.; Gin, D. Y.; Gin, M. S. *J. Am. Chem. Soc.* **2004**, *126*, 1638–1639.
 (37) Kikuzawa, A.; Kida, T.; Akashi, M. *Org. Lett.* **2007**, *9*, 3909–3912.
 (38) Kikuzawa, A.; Kida, T.; Akashi, M. *Macromolecules* **2008**, *41*, 3393–3395.
 (39) Takeo, K.; Shinmitsu, K. *Carbohydr. Res.* **1984**, *133*, 135–145.
 (40) Blanc-Muesser, M.; Driguez, H.; Lehmann, J.; Steck, J. *Carbohydr. Res.* **1992**, *223*, 129–136.
 (41) Dong, H.; Pei, Z.; Ramstrom, O. *J. Org. Chem.* **2006**, *71*, 3306–3309.
 (42) Varela, O.; Cicero, D.; Lederkremer, R. M. *J. Org. Chem.* **1989**, *54*, 1884–1890.
 (43) Gamblin, D. P.; Garnier, P.; van Kasteren, S.; Oldham, N. J.; Fairbanks, A. J.; Davis, B. G. *Angew. Chem., Int. Ed.* **2004**, *43*, 828–833.
 (44) Yu, H. N.; Ling, C. C.; Bundle, D. R. *J. Chem. Soc., Perkin Trans. 1* **2001**, 832–837.
 (45) Schneider, H. J.; Hacket, F.; Rüdiger, V.; Ikeda, H. *Chem. Rev.* **1998**, *98*, 1755–1786.
 (46) Saenger, W.; Jacob, J.; Gessler, K.; Steiner, T.; Hoffmann, D.; Sanbe, H.; Koizumi, K.; Smith, S. M.; Takaha, T. *Chem. Rev.* **1998**, *98*, 1787–1802.
 (47) Gessler, K.; Usón, I.; Takaha, T.; Krauss, N.; Smith, S. M.; Okada, S.; Sheldrick, G. M.; Saenger, W. *Proc. Natl. Acad. Sci. U.S.A.* **1999**, *96*, 4246–51.
 (48) French, A. D.; Johnson, G. P. *Carbohydr. Res.* **2007**, *342*, 1223–1237.
 (49) Keepers, J. W.; James, T. L. *J. Magn. Reson.* **1984**, *57*, 404–426.
 (50) Thomas, P. D.; Basus, V. J.; James, T. L. *Proc. Natl. Acad. Sci. U.S.A.* **1991**, *88*, 1237–1241.
 (51) Tvaroska, I.; Hricovini, H.; Petrakova, E. *Carbohydr. Res.* **1989**, *189*, 359–362.
 (52) Mulloy, B.; Frenkiel, T. A.; Davies, D. B. *Carbohydr. Res.* **1988**, *184*, 39–46.
 (53) Cloran, F.; Carmichael, I.; Serianni, A. S. *J. Am. Chem. Soc.* **1999**, *121*, 9843–9851.
 (54) Steiner, T.; Koellner, G. *J. Am. Chem. Soc.* **1994**, *116*, 5122–5128.
 (55) Naidoo, K. J.; Gamielien, M. R.; Chen, J. Y.; Widmalm, G.; Maliniak, A. *J. Phys. Chem. B* **2008**, *112*, 15151–15157.
 (56) Wormald, M. R.; Petrescu, A. J.; Pao, Y. L.; Glithero, A.; Elliott, T.; Dwek, R. A. *Chem. Rev.* **2002**, *102*, 371–386.
 (57) Tan, X.; Lindenbaum, S. *Int. J. Pharm.* **1991**, *74*, 127–135.
 (58) Yang, Z.; Breslow, R. *Tetrahedron Lett.* **1997**, *38*, 6171–6172.
 (59) Cabrer, P. R.; Alvarez-Parrilla, E.; Meijide, F.; Seijas, J. A.; Núñez, E. R.; Tato, J. V. *Langmuir* **1999**, *15*, 5489–5495.
 (60) Movileanu, L.; Cheley, S.; Bayley, H. *Biophys. J.* **2003**, *85*, 897–910.
 (61) Khan, A. R.; Forgo, P.; Stine, K. J.; D'Souza, V. T. *Chem. Rev.* **1998**, *98*, 1977–1996.
 (62) Hinrichs, W.; Saenger, W. *J. Am. Chem. Soc.* **1990**, *112*, 2789–2796.
 (63) Saenger, W.; Niemann, C.; Herbst, R.; Hinrichs, W.; Steiner, T. *Pure Appl. Chem.* **1993**, *65*, 809–817.
 (64) Gattuso, G.; Nepogodiev, S. A.; Stoddart, J. F. *Chem. Rev.* **1998**, *98*, 1919–1958.
 (65) Thornton, J. M. *J. Mol. Biol.* **1981**, *151*, 261–287.
 (66) Quiocio, F. A. *Annu. Rev. Biochem.* **1986**, *55*, 287–315.
 (67) Bush, C. A.; Martin-Pastor, M.; Imbert, A. *Annu. Rev. Biophys. Biomol. Struct.* **1999**, *28*, 269–293.
 (68) Aachmann, F. L.; Otzen, D. E.; Larsen, K. L.; Wimmer, R. *Protein Eng.* **2003**, *16*, 905–912.
 (69) Sujatha, M. S.; Sasidhar, Y. U.; Balaji, P. V. *Biochemistry* **2005**, *44*, 8554–8562.
 (70) Brandl, M.; Weiss, M. S.; Jabs, A.; Sühnel, J.; Hilgenfeld, R. *J. Mol. Biol.* **2001**, *307*, 357–377.
 (71) Thrippleton, M. J.; Keeler, J. *Angew. Chem., Int. Ed.* **2003**, *42*, 3938–3941.
 (72) Edden, R. A. E.; Keeler, J. *J. Magn. Reson.* **2004**, *166*, 53–68.
 (73) Hwang, T.-L.; Shaka, A. J. *J. Am. Chem. Soc.* **1992**, *114*, 3157–3159.
 (74) Montal, M.; Mueller, P. *Proc. Natl. Acad. Sci. U.S.A.* **1972**, *69*, 3561–3566.